Principles of Meiotic Chromosome Assembly

*Stephanie A. Schalbetter[1], *Geoffrey Fudenberg[2], Jonathan Baxter[1], Katherine S. Pollard[2,3,4], and Matthew J. Neale[1]

*SAS and GF contributed equally to this work

1. Genome Damage and Stability Centre, School of Life Sciences, University of Sussex, UK
2. Gladstone Institute of Data Science and Biotechnology, San Francisco, USA
3. Department of Epidemiology & Biostatistics, Institute for Human Genetics, Quantitative Biology Institute, and Institute for Computational Health Sciences, University of California, San Francisco, California, USA.
4. Chan-Zuckerberg Biohub, San Francisco, California, USA.

Abstract

During meiotic prophase, chromosomes organise into a series of chromatin loops emanating from a proteinaceous axis. Yet, while much is known about meiotic chromosome morphology, the mechanism of assembly, and how assembly is regulated, remain open questions. Here we combine genome-wide chromosome conformation analysis (Hi-C) with *Saccharomyces cerevisiae* genetics and *in silico* polymer modelling to elucidate the mechanisms that shape meiotic chromosomes. Entering meiosis, grid-like Hi-C interaction patterns emerge that correspond to the localisation of—and depend upon—the meiotic cohesin subunit Rec8. Such patterns fit a model of loop extrusion, where a heterogeneous population of expanding loops develop along the chromosome, with growth limited by barriers. While grid-like patterns emerge independently of chromosome synapsis, synapsis itself generates additional compaction that matures differentially depending on telomeric distance and chromosome size. Our results elucidate fundamental principles of meiotic chromosome assembly and demonstrate the essential role of cohesin within this evolutionarily conserved process.

Introduction and results

During meiosis, eukaryotic chromosomes are broken, repaired and paired with their homologs followed by two rounds of segregation—a series of events accompanied by dynamic structural changes of the chromosomes. Most prominent is the arrangement of pachytene chromosomes into a dense array of chromatin loops emanating from a central proteinaceous core, the synaptonemal complex (SC), which is highly conserved across eukaryotes[1,2]. In *S. cerevisiae*,

1

35   SC components include the meiotic cohesin kleisin subunit, Rec8[3], the transverse filament,

36   Zip1[4], the axial/lateral elements, Hop1 and Red1[5,6], and the pro-DSB factors Rec114-Mei4-

37   Mer2 (RMM)[7,8]. Much of our understanding of meiotic chromosome structure has been deduced

38   from a combination of electron microscopy, immunofluorescence microscopy, and the genome-

39   wide patterns of protein localisation determined by ChIP. However, the link between key meiotic

40   protein complexes, chromosome conformation, and genomic sequence remains

41   uncharacterized.

42

43   Chromosome conformation capture (3C) techniques generate maps of pairwise contact

44   frequencies that are snapshots of chromosome organisation. 3C methods were originally

45   applied to assay chromosome conformation in *S. cerevisiae*, including during meiosis[9]. Now

46   they are widely used across a range of organisms and cellular contexts to link 3D organisation

47   directly with genomic sequence[10], revealing important roles of the Structural Maintenance of

48   Chromosomes (SMCs) cohesin and condensin in genomic organization[11,12], where they likely

49   mediate chromosome compaction via the process of loop extrusion[13]. Here we return to yeast

50   meiosis to interrogate genome-wide chromosome organisation by Hi-C, elucidate mechanisms

51   of chromosome assembly, and define the role of key meiotic chromosome components,

52   including cohesin and the SC.

53

54   Starting with a synchronized G1 population we analysed timepoints encompassing DNA

55   replication, meiotic prophase and both meiotic divisions (**Fig. 1a,b,c, Extended Data Fig.**

56   **1a,b,c**). In G1, we detect strong centromere clustering (**Fig. 1a,d**) and folding back of the arms

57   at the centromeres (**Fig. 1a, Supplementary Fig. 2**), characteristic of a Rabl conformation[9,14].

58   During meiosis, centromere clustering is transiently dissolved (3-5h, **Fig. 1a,d, Extended Data**

59   **Fig. 1a**); this coincides with a global decrease in inter-chromosomal contact frequency at mid-

60   prophase, reflecting chromosome individualisation. Subtelomeric clustering also decreases

61   during meiotic prophase (**Fig. 1a,d, Extended Data Fig. 1a**), with no evidence for the transient

62   telomeric bouquet conformation, consistent with prior microscopic analyses[15].

63

64   Entering meiosis, contact frequency versus distance, *P(s),* curves display a shoulder, consistent

65   with the linear compaction of chromosome arms increasing due to *cis*-loop formation (2-4h, **Fig.**

66   **1e, Extended Data Fig. 1d**, e.g. as defined[16]; for review[13]). This change in *P(s)* is reminiscent

67   of the SMC-dependent changes observed via Hi-C during mitosis across species[17–21].

68   Compaction coincides with meiotic prophase I and the formation of the SC at pachytene, and is

69   lost at later stages (**Fig. 1e, Extended Data Fig. 1d**).

70

71   To study meiotic chromosome conformation in more detail, and to eliminate cell-to-cell
72   heterogeneity (**Fig. 1b,c**), we enriched for pachytene cells in subsequent experiments by
73   inactivating Ndt80, a transcription factor required for exit from meiotic prophase[22]. *ndt80Δ* cells
74   enter meiosis synchronously, assessed by bulk DNA replication (**Fig. 1f**), but do not initiate the
75   first nuclear division[22]. Similar to the wild type prophase population (3-5 h), but likely
76   accentuated by the increased homogeneity, Hi-C maps of pachytene-enriched cells displayed
77   total loss of centromere clustering (**Extended Data Fig. 2**) and dramatic chromosome arm
78   compaction (**Fig. 1e**). Analysing compaction in more detail, shorter chromosomes (**Extended
79   Data Fig. 1e**) and, in particular, shorter chromosome arms (**Fig. 1h, Extended Data Fig. 1f**),
80   displayed elevated contact frequency at short genomic separations, and an earlier shoulder,
81   apparently arising from distinct behavior of subtelomeric and subcentromeric regions (**Fig. 1h,
82   Extended Data Fig. 1g**). Moreover, distinct *P(s)* for chromosomes with different length arms
83   (**Extended Data Fig. 1h**) suggests that the centromere can insulate the process that leads to
84   differences between arms. In agreement with this, compaction is interrupted at centromeres in
85   Hi-C maps (**Fig. 1a**, **Extended Data Fig. 2b**).

86

87   Zooming in to consider within-arm organisation revealed punctate grid-like Hi-C interactions
88   between pairs of loci during prophase (**Fig. 2a**), particularly prominent in *ndt80Δ* (**Fig. 2a,b**).
89   Such patterns have not been observed in yeast[19,21], human[20,23], or chicken[17] mitotic
90   chromosomes, which all display locus-independent compaction along chromosome arms. The
91   focal meiotic patterns we observe are more prominent than reported previously[24]— resembling
92   peaks between CTCF sites[25] rather than topological domains[26,27] detected in mammalian
93   interphase Hi-C maps—and likely arise from a heterogeneous mixture of 'transitive' interactions
94   and 'skipping' of peak bases (**Fig. 2c**).

95

96   Genomic regions underlying the punctate Hi-C interactions display a remarkable visual (**Fig.
97   2a,b**), and quantitative (**Fig. 2d-g**), correspondence with previously characterised sites of high
98   Rec8 occupancy[28]. At pachytene, Rec8 sites display elevated *cis*/total contact frequencies (**Fig.
99   2d**), enriched contact frequency (**Fig. 2e,f**), and evidence of insulation (**Fig. 2g**)—features that
100 correlate with Rec8 occupancy measured by ChIP (**Fig. 2a, lower**). In wild type cells, Rec8-
101 Rec8 interactions became visible in early prophase (2 h) peaked at mid prophase (4 h), and
102 were especially prominent in the homogenous *ndt80Δ* cell population (**Fig. 2a-g, Extended
103 Data Fig. 4b,c**). Importantly, Rec8-Rec8 enrichments are strongest between adjacent sites,
104 decrease between non-adjacent sites with increasing genomic separation, and are absent in
105 *trans* (**Extended Data Fig. 4b,c**). As for enrichments between CTCF sites in mammalian

106 interphase[29], these observations argue that a cis-acting process generates such focal
107 interactions in meiosis.

108

109 Rec8 is a central component of the meiotic chromosome axis[3]. Assaying a *rec8Δ* mutant
110 enabled us to determine that Rec8 is absolutely required for the emergence of the grid-like Hi-
111 C patterns present in meiosis (**Fig. 2a,b**). Moreover, *rec8Δ* cells completely lose the shoulder
112 in *P(s)*, indicative of a dramatic loss of arm compaction (**Fig. 2b, Extended Data Fig. 4a**), similar
113 to that caused by depletion of SMCs in diverse contexts[17,19,21,30–32]. Instead of assembling an
114 axis of loops, *rec8Δ* cells appear to be caught in a state with highly clustered telomeres
115 (**Extended Data Fig. 4d, Extended Data Fig. 3**), consistent with previous observations by
116 microscopy[33,34]. Moreover, in *rec8Δ* cells *cis* contact frequency is reduced (**Fig. 2d**), similar to
117 G1 cells, and cis/total no longer correlates with Rec8 occupancy. Instead, *rec8Δ* cis/total
118 displays a decreasing trend along chromosome arms, likely due to persistent telomere
119 clustering (**Extended Data Fig. 4d**).

120

121 To test how compaction and grid-like interaction patterns could jointly emerge in meiosis, we
122 developed polymer simulations (**Fig. 3a, Methods**) similar to those used to successfully
123 describe the assembly of TADs in mammalian interphase chromosomes[13]. Importantly, these
124 simulations employ the *cis*-acting process of loop extrusion, where extruders dynamically form
125 progressively larger chromatin loops, unless impeded by adjacent extruders or barrier elements
126 (**Fig. 3a**). Because the accumulation of Rec8 at ChIP-seq sites[28] concomitant with convergent
127 transcription[35] is indicative of barriers to extrusion[29], we positioned bi-directional barriers at Rec8
128 sites.

129

130 Simulations were used to explore variations in loop extrusion dynamics to determine whether
131 specific parameter combinations are able to generate Hi-C maps that agree with experimental
132 observation (**Fig. 3, Methods**). Models with excellent fits were identified in which ~65% of the
133 genome is covered by extruded loops (**Fig. 3b,c, Extended Data Fig. 5**)—a far denser array
134 than present in *S. cerevisiae* mitosis[21], but still less compact than human mitotic cells[20]. Even
135 though extrusion can generate compaction independently of barriers (**Fig. 3d**), an intermediate
136 barrier strength is essential to match the grid-like patterns observed experimentally (**Fig. 3b**).
137 Despite the simplifying assumptions, simulated chromosomes displayed many features
138 observed experimentally: (i) chromosomes fold into a loose polymer brush[3,36,37], with a Rec8-
139 rich core[3] (**Fig. 3f, Extended Data Fig. 5a**); (ii) a grid-like interaction pattern naturally emerges
140 in simulated Hi-C maps (**Fig. 3d**); (iii) importantly, because loop extrusion is a *cis*-acting

141 process, pairs of Rec8 sites at increasing separations naturally have lower contact frequency
142 (**Fig. 3e**).

143

144 Simulations also highlight the stochasticity of loop positions across the cell population, with most
145 barriers (73%) unoccupied by an extruder, and extruders paused with barrier elements on both
146 sides only a minority of the time (15%) in the best fitting models (**Extended Data Fig. 6c**).
147 Because of this, the majority (65%) of extruded loops cross over Rec8 sites, consistent with an
148 average loop size roughly twice the average distance between Rec8 ChIP peaks (26 kb versus
149 12 kb, **Extended Data Fig. 6d**), and remarkably consistent with estimates made using EM
150 (~20kb[36]). Most strikingly—despite the prominence of Rec8-dependent grid-like features in the
151 experimental data (**Fig. 2c**)—our simulations indicate that Rec8 sites are not always occupied
152 by extruding cohesins and thus are present at the meiotic chromosome core in only a subset of
153 cells, as inferred previously[38].

154

155 The range of loop extrusion parameters we explored encompasses the situation where Rec8
156 sites always halt extrusion and *cis*-loops are formed between each consecutive Rec8 site.
157 However, simulations with these parameters have quantitatively poor fits with experimental
158 maps (**Fig. 3d-e, ii**): the bend in *P(s)* comes too early to recapitulate experimental *P(s)*, and
159 Rec8-Rec8 contacts are much too strong. The poor fit of such 'direct-bridging' simulations
160 underscores the conclusion that only a fraction of Rec8 sites are occupied in a given cell, and
161 argues that cohesin-dependent *cis*-loops must link regions that are not primary Rec8 binding
162 sites in order to provide compaction without making Rec8-Rec8 enrichments overly strong.

163

164 A crucial prediction of our loop extrusion simulations is that depletion of extruders in meiosis
165 would lead to both decompaction and loss of the grid-like pattern of Hi-C interactions. When we
166 repeated our fitting procedure for *rec8Δ*, the best fits were for simulations with either no, or very
167 few, extruded loops (**Extended Data Fig. 5e**). The lack of compaction in these simulations
168 (**Extended Data Fig. 5a**) is consistent with previous EM showing decompacted chromatids in
169 *rec8Δ*[3]. Such joint consistency between Hi-C and imaging data further supports loop extrusion
170 as a mechanism underlying assembly of the cohesin-rich core and contributing to chromosomal
171 compaction in meiosis. Our simulations also open the possibility that overly-shortened axes
172 observed upon Wapl[39,40] and Pds5[41] depletion may reflect heightened extruder processivity[42]
173 upon which shortened SCs are assembled, and predict that such perturbations would cause a
174 rightward shift in the *P(s)* shoulder measured via Hi-C (**Extended Data Fig. 5c**).

175

To investigate how homologue synapsis affects chromosome conformation, we assayed pachytene cells in the absence of Zip1, the transverse filament of the SC[4], and Hop1, an axial element required for Zip1 loading[6] (**Fig. 4a,b**). Both *zip1*Δ and *hop1*Δ Hi-C maps retained the Rec8-dependent punctate interactions (**Fig. 4b, Extended Data Fig. 2b,c**), and displayed compaction relative to G1 or *rec8*Δ, but with the *P(s)* shoulder shifted left relative to *ndt80*Δ (**Fig. 4c**). Attempts to model the known *zip1*Δ and *hop1*Δ defects in chromosome synapsis simply by removing interhomologue crosslinks from best-fitting *ndt80*Δ simulations did not recapitulate the *P(s)* shift observed experimentally (**Extended Data Fig. 5f**), consistent with the suggestion that interhomologue contacts make only a minor contribution within meiotic Hi-C maps[24]. Instead, best-fitting simulations had shifts towards slightly lower processivity and larger separation, consistent with less axial compaction relative to the *ndt80*Δ control (**Fig. 4e**). Interestingly, subtelomeric regions no longer displayed a distinct *P(s)* in *zip1*Δ and *hop1*Δ (**Fig. 4d**), suggesting that chromosome compaction at chromosome termini is regulated differentially.

Discussion

Our analysis of meiotic chromosome organisation reconciles the function and localisation of factors thought to shape meiotic chromosomes with their 3D organisation. Crucially, we have demonstrated the centrality of cohesin function and localisation for meiotic *cis*-loop formation—formally demonstrating the link between preferential positioning of Rec8 along the genome[28,35] and the inference that these loci come into close proximity based on the localization of Rec8 to the chromosomal axes[3].

Rec8 positioning correlates with sites of converging transcription[35]. We favour the view that transcription acts as a barrier to cohesin-dependent loop extrusion in meiosis, rather than as a motive force as previously proposed[35], consistent with transcription-independent compaction by cohesin in mammalian interphase[43] and direct observation of extrusion by the related SMC condensin *in vitro*[44]. Nevertheless, whether barriers arise directly from Pol2 binding, or indirectly via other axis proteins, remains to be determined. Loop extrusion would also be expected to be blocked by large DNA-protein complexes[29], such as the kinetochore—consistent with the paucity of Rec8-dependent loops that span the centromere.

Our simulations also help reveal a nuanced picture of meiotic chromosome assembly: loops are, on average, larger than the inter-Rec8 peak distance, and more than half of the loop bases are not associated with preferred sites of Rec8 binding. Moreover, it is likely that loop sizes and positions vary widely from one cell to another, making classifications of genomic regions as 'axis' or 'loop' a great oversimplification. Despite using the simplifying assumption that all

barriers had equal strength, our simulations generated interaction maps closely resembling experimental Hi-C maps. This agreement furthers the case for loop extrusion as a general mechanism[19–21,24,29,45–48] that is flexibly employed and regulated in interphase, mitosis, and meiosis.

Our results point to interesting similarities and differences between yeast mitosis and meiosis. In both systems, chromosome arm compaction is dependent on the corresponding cohesin kleisin subunit and consistent with *cis*-loops generated via loop extrusion. The presence of focal interactions in meiosis but not in mitosis remains intriguing, however, and suggests the influence of additional components. Indeed, loop extrusion simulations require barriers to agree with experimental meiotic Hi-C maps. Nevertheless, our observations enable us to rule out the axial element, Hop1, the SC transverse filament, Zip1, and the process of homologous recombination mediated by Spo11, Sae2, and Dmc1 (unpub. obs.) as important for the generation of such patterns.

It is notable that the meiotic grid-like pattern of interactions observed between Rec8 sites is reminiscent of the patterns seen between oriented CTCF sites in mammalian interphase[13,25]. Interestingly, the meiotic patterns are even more reminiscent of the Hi-C patterns observed in interphase mammalian cells upon depletion of the cohesion unloader, Wapl[32,43], wherein "vermicelli"-like chromatids arise with a cohesin-rich backbone[49], suggesting that cohesin metabolism may be altered in meiosis via modulation of the cohesin regulators.

Our results also reveal how the interplay between the synapsis components, Hop1 and Zip1, influences chromosome morphology. That Hop1 and Zip1 are both required to increase chromosome compaction at pachytene likely points at their joint role in promoting synapsis[4,6], and supports the view that synapsis itself modulates axial compaction. Interestingly, whilst Zip1 binds largely uniformly along the arms of pachytene chromosomes[50], subtelomeres and short chromosomes display an increase in short-range contacts and an earlier shoulder in *P(s)*, consistent with smaller loops or less compression of spacers between loops in these regions, and therefore less axial compaction. Because such differences correlate with disproportionate retention of Hop1 in these regions[50] and diminished efficiency of synapsis[51], it is possible that Hop1 impedes the pathway whereby Zip1 imposes additional compaction upon synapsis. Nevertheless, it is unclear whether Zip1 mediates this effect by modifying loop extrusion dynamics, or via a distinct process of axial compression, as has been argued for higher-eukaryote mitotic chromosome compaction[20]. Given the influence that chromosome structure has over so many aspects of meiosis, teasing apart these mechanisms is of great future interest.

247

Acknowledgements & Contributions

Data & Code Availability

All processed Hi-C matrices are publicly accessible via the interactive HiGlass[52] viewer. Live web links are provided with each figure. Raw sequence reads will be made publicly accessible via the SRA repository upon final publication. Code for data analysis is either already publicly available online or will be made available on request or via Github upon final publication.

Figure Legends

Figure 1. Chromosome conformation during yeast meiosis.

a. Cells were collected during meiosis at indicated timepoints and analysed by Hi-C. At 0h the cells are in G1. Representative Hi-C contact maps of chromosomes 6, 11, and 7 plotted at 5 kb resolution. Centromeres, telomeres and arm fold-back at the centromere are indicated by blue, red and grey arrows, respectively, and axial compaction by the width of the main diagonal relative to the fixed-width black clamp. For interactive HiGlass[52] views see: http://higlass.pollard.gladstone.org/app/?config=Z5iwKpjzQpePCXXyvuYGeQ

b. Meiotic entry assessed by FACS; at 4 h, the majority of cells show a 4C peak indicating completion of DNA replication.

c. Meiotic progression was monitored by quantification of nuclear divisions determined by DAPI staining. Around 4 h, cells start to undergo meiotic divisions I and II. The majority of cells undergo meiotic divisions between 4 and 8 h, indicating the degree of heterogeneity within the cell population.

d. *Upper panels*: Average *trans* centromere-centromere contact maps. *Lower panels*: *trans* telomere-telomere contact maps. *Right*: ratio of *cis* to total contact frequency.

e. Intra-arm contact probability versus genomic distance, *P(s),* indicating the emergence (*left*) and disappearance (*right*) of chromosome arm compaction during meiosis. Shaded area bounded above and below by the two *ndt80Δ* 8h replicates.

f. Meiosis was induced in *ndt80Δ* cells for 8h and meiotic entry was checked by monitoring DNA replication by FACS.

g. *ndt80Δ* cells were grown for 8h in sporulation media and analysed by Hi-C (*left*). Log2 ratio of *ndt80Δ* cells 8h over G1 (*right*). Centromeres and telomeres are indicated by blue and red arrows, respectively, and axial compaction by a black clamp.

h. *Left*: Contact probability of individual chromosome arms stratified by length. *Right*: Contact probability stratified by the distance from the telomere.

Figure 2. Emergence of a Rec8-dependent grid of punctate interactions in meiosis

a. Hi-C contact maps of chromosome 11 for the indicated genotypes plotted at 2 kb bin resolution, showing near-diagonal interactions. Wild type timepoints as in **Fig. 1a**. **Lower panels**: log2(insulation); cis/total ratio, Rec8 ChIP-seq[28], all binned at 2kb. Insulation and cis/total calculated from *ndt80Δ* maps. Positions of Rec8 sites indicated as green circles. Genome-wide cis/total (Spearman's R=0.62, P<1e-10) and insulation (R= -0.23, P<1e-10, insulation window = 20 kb) profiles are correlated with Rec8 occupancy.

b. Zoom-in into contact maps on chromosome 11 (0-200kb) of wt-4h and *ndt80Δ* (top) and *rec8Δ* (*bottom left*). Contact probability versus genomic distance, *P(s)*, for G1(*ndt80Δ-0h*) and *ndt80Δ* and *rec8Δ* (*bottom right*). Data shown is the average (n=2) except for wt-4h. Rec8 peak sites called from ChIP-seq data[28] are indicated in green. For an interactiveview see: http://higlass.pollard.gladstone.org/app/?config=Twrh61jGT4SlxotaguTIJg

c. Simplified illustration of how a grid of peaks on a Hi-C map can emerge between Rec8 sites either by transitive contacts between adjacent loops, or by loops that skip over adjacent sites. Experimentally observed grids extend much further than separation=2 (**Extended Data Fig. 4c**)

d. Cis/total ratios for Rec8 (green) and nonRec8 (grey) sites for indicated datasets.

e. Contact frequency versus distance between Rec8-Rec8 sites (green), Rec8-nonRec8 sites (light green) and nonRec8-nonRec8 sites (green).

f. Log2 ratio of contact frequency between adjacent Rec8-sites (separation=1) compared to average cis interactions.

g. Log2 ratio of contact frequency centered at Rec8 sites compared to average cis interactions.

307   In *ndt80Δ*, Rec8 sites show: elevated cis/total frequency (0.85 versus 0.77), elevated

308   pairwise contact frequency (~2-fold at 20 kb), and mild insulation. These distinctions are similar in wild

309   type pachytene (4h) yet absent in G1 (*ndt80Δ-0h*) or in *rec8Δ*.

Figure 3. Model for meiotic chromosome compaction in prophase.

310

311   **a.** In simulations, yeast chr13 was represented as a polymer fiber confined to the nucleus

312   subject to additional meiosis-specific constraints. These include: extruded loops, sister

313   crosslinks, and homolog crosslinks (**Methods**). Barriers to extruded loops were placed at Rec8

314   sites[28]. We imposed inter-sister and inter-homologue crosslinks at sites of extruded loop bases

315   in order to approximate the paired arrangement of homologues at pachytene (**Extended Data**

316   **Fig. 6**). For each set of extruded loop parameters (*processivity, separation,* and *barrier*

317   *strength*), conformations were collected and used to generate simulated contact maps. These

318   were then compared with experimental contact maps via the combined average fold

319   discrepancy with *P(s)* curves for Rec8-Rec8, Rec8-non, and non-non bin pairs at 2 kb

320   resolution.

321   **b.** Goodness-of-fit for indicated barrier strengths over coarse grids of processivity and

322   separation demonstrate that intermediate barrier strengths are required to agree with

323   experimental *ndt80Δ* Hi-C maps.

324   **c.** Goodness-of-fit for a fine grid of processivity versus separation at barrier strength 0.95. Best-

325   fitting models had separation ~32kb and processivity ~76kb, corresponding to ~60% coverage

326   of the genome by extruded loops of average length 26kb.

327   **d.** From *left* to *right*: contact maps for chr13 for *ndt80Δ*, and simulations with (i) best-fitting

328   parameters, (ii) relatively stable loops between neighboring Rec8 sites, and (iii) no barriers.

329   **e.** P(s) split by Rec8-Rec8, Rec8-non, and non-non, as in **Fig. 2D**.

330   **f.** Conformations for best-fitting simulations, which highlight: (*left)* one chromatid colored from

331   start (red) to end (blue); *(right*) extruders (yellow), extrusion barriers (red), and extruders paused

332   at barriers (orange).

Figure 4. Hop1 and Zip1-dependent compaction of Rec8-dependent loops.

333

334   **a.** *Top*: Hi-C maps for *hop1Δ* and *zip1Δ* (plotted as in **Fig. 1a**). *Bottom*: Log2 ratio of hop1Δ over

335   *ndt80Δ* (as in **Fig. 1g**). For interactive views of the full genome, see

336   http://higlass.pollard.gladstone.org/app/?config=TTBGu5DDR0SHAa09zrjTXA

337   **b.** Hi-C contact maps of chromosome 11 for *hop1Δ* and *zip1Δ* plotted at 2kb bin resolution,

338   showing near-diagonal interactions, as in **Fig. 2a**.

339 **c.** Contact probability versus genomic distance for G1, *ndt80Δ*, *hop1Δ*, *zip1Δ*. Shaded area

340 bounded above and below by *ndt80Δ* replicas. Average between two replicas for *zip1Δ* and one

341 sample for G1 and *hop1Δ* are shown.

342 **d.** Contact probability over genomic distance averaged over all chromosome arms stratified by

343 distance from the telomere.

344 **e.** Goodness-of-fit for simulations without homolog crosslinks with a fine grid of processivity

345 versus separation at barrier strength 0.95 *zip1Δ* and *hop1Δ*.

346 **f.** Model of meiotic chromosome compaction: Rec8-dependent loop formation leads to initial

347 chromosome arm compaction and emergence of a grid-like pattern of Hi-C interactions that

348 jointly agrees with a mechanism of loop extrusion including barrier elements. We suggest that

349 transcription could impose such barriers. Hop1 and Zip1 are dispensable for this step, but are

350 required for synapsis, where additional compaction occurs differentially along chromosome

351 arms.

352

353 **Extended Data Fig. 1**

354 **a-d.** Results from a replicate timecourse, collected and characterized independently of the

355 timecourse in Fig. 1.

356 **a.** Hi-C maps, plotted as in Fig. 1a.

357 **b.** FACS as in Fig. 1b.

358 **c.** DAPI as in Fig. 1c.

359 **d.** *P(s)* as in Fig. 1e.

360 **e.** *P(s)* for chromosomes stratified by size for *ndt80Δ*-0h, *ndt80Δ*-8h. Short chromosomes

361 display relatively elevated *P(s)* at short distances, and an earlier shoulder.

362 **f.** *Left*: *P(s)* for individual chromosome arms, stratified by size for wt-4h. Short arms display

363 relatively elevated *P(s)* at short distances, and an earlier roll-over. *Right*: Intra-arm *P(s)* stratified

364 by the distance from the telomere for wt-4h, averaged across all chromosomes. Telomere-

365 proximal regions display elevated *P(s)* at short distances.

366 **g.** Intra-arm *P(s)* stratified by the distance from the centromere for G1 (*ndt80Δ*-0h), *wt*-4h,

367 *ndt80Δ*-8h, averaged across all chromosomes.

368 **h.** Contact probability of single chromosome arms for *ndt80Δ*-8h.

369 **Extended Data Fig. 2**

370 **a.** Average *trans* centromere-centromere contact maps for indicated data sets.

371 **b.** Average *cis* centromere-centromere contact maps for indicated data sets. Note the loss of

372 the folding back in meiosis, and how the intra-arm enrichment is insulated at centromeres in

373 meiosis.

Extended Data Fig. 3

a. Average *trans* telomere-telomere contact maps for indicated datasets.

b. Average telomere-telomere contact maps between the two telomeres of the same chromosome.

c. Average contact map around each telomere in *cis.*

Extended Data Fig. 4

a. *Left*: Hi-C contact maps of *rec8Δ ndt80Δ*. Chromosomes 6, 11 and 7 are shown as representatives for the whole genome. *Right*: Log2 Hi-C ratio maps of *rec8Δ ndt80Δ / ndt80Δ*. Plotted as in Fig. 1g.

b. Log2 observed over expected contact frequency at Rec8-Rec8 peak pairs as a function of separation across datasets.

c. Log2 observed over expected contact frequency +/-8kb around Rec8-Rec8 peak pairs at the indicated separations.

Together, **b-c** demonstrate that Rec8-Rec8 enrichments are strongest between adjacent sites, decrease between non-adjacent sites with increasing genomic separation, and are absent in *trans*. Equally important, these meiotic features are lost in *rec8Δ*. As for mammalian interphase, this observation in meiosis argues for a *cis*-acting process underlying the formation of focal interactions between Rec8 sites.

d. cis/total as a function of distance along the chromosomal arm, Rec8 sites marked in green.

Extended Data Fig. 5

a. Representative conformation for the indicated parameter sets. As in **Fig. 3f,** one chromatid from a homologous quartet of chromatids coloured from start to end according to the spectrum; other three coloured in grey.

b. For the same three conformations, positions of Rec8 sites indicated with red spheres, positions of extruded loop bases in yellow, and extruders overlapping a Rec8 site in orange. Note the stable loops between neighbouring Rec8 sites creates a very elongated chromatid (ii). Also note the majority of Rec8 sites are unoccupied in (iii), despite the self-assembly of two axial cores and a strong brush. Finally, note very dispersed chromosomes in (iv), consistent with EM[3] for *rec8Δ.*

c. Contact frequency versus distance, *P(s),* for indicated simulations. Note that the loss of the shoulder in *P(s)* in the case of full extruder depletion mirrors the difference between experimental *ndt80Δ* and *rec8Δ* Hi-C maps. Simulations with increased processivity predict that *P(s)* would shift rightward if unloading was impaired, as could happen in *waplΔ.* Conversely, if

unloading was enhanced, simulations with decreased processivity indicate a leftward shift in P(s), until the absence of extruders.

d. Goodness-of-fit for a fine grid of processivity versus separation at barrier strength 0.90. The best-fit occurs at similar processivity and separation as for barrier strength 0.95 shown in **Fig. 3c**, but with slightly lower goodness-of-fit.

e. Goodness-of-fit to *rec8Δ* data for simulations with the indicated barrier strengths (in grey: 0.00, 0.75, 0.90, 0.95, 0.99, 1.00) over coarse grids of processivity and separation demonstrates that the best fits have few if any extruded loops, regardless of barrier strength.

f. *P(s)* curves for simulations with sisters and homologs with the best-fitting parameters for *ndt80Δ-8h* maps compared to P(s) for simulations with sisters only show that simply removing homolog tethering does not recapitulate the sort of shifted P(s) seen experimentally in *zip1Δ* Hi-C.

Extended Data Fig. 6

a. Simulated contact maps for the indicated region of chr13 for: (i) best-fitting simulations, (ii) simulations with relatively stable loops between neighboring Rec8 sites (barrier strength=1 and high processivity), and (iii) no barriers, as in **Fig. 2d.**

b. Simulated ChIP-seq profiles for the indicated region of chr13. Best-fitting simulations (i) display occupancy well below 100% at Rec8 sites. Simulations with stable loops (ii) display highly occupied Rec8 sites. Simulations without barriers (iii) have homogenous Rec8 occupancy across the genome.

c. Positions of extruded loops (arcs) sister crosslinks (solid black lines) and homolog crosslinks (dashed lines) for four chromatids in two separate cells, showing how the simulated Hi-C maps and ChIP-seq profiles emerge from the stochastic positioning of extruded loops from cell-to-cell. For statistics, see **Supplementary Table S1**.

d. Histogram of extruded loop lengths for indicated parameters (i, ii, iii).

Tables

Table 1. *S. cerevisiae* strains used in this study

Strain name	Genotype
MJ6	*ho::LYS2/", lys2/", ura3/", arg4-nsp/", leu2::hisG/", his4X::LEU2/", nuc1::LEU2/"*

SSY14	*ho::LYS2/", lys2/", ura3/", arg4-nsp/", leu2::hisG/", his4X::LEU2/", nuc1::LEU2/", ndt80Δ::LEU2/"*
SSY20	*ho::LYS2/", lys2/", ura3/", arg4-nsp/", leu2::hisG/", rec8Δ::KanMX4/", ndt80Δ::LEU2/"*
SSY25	*ho::LYS2/", lys2/", ura3/', arg4-nsp/", leu2::hisG/", his4X::LEU2/", nuc1::LEU2/", zip1::LEU2/", ndt80Δ::LEU2/"*
SSY49	ho::LYS2/", lys2/", ura3/", arg4-nsp/", leu2::hisG/", nuc1::LEU2/", his4X::LEU2/", hop1::LEU2/", ndt80Δ::LEU2/"
SSY58	ho::hisG/", lys2/", ura3/", leu2::hisG/", nuc1::LEU2/", arg4-nsp/", rec8::KanMX/", ndt80Δ::LEU2/"

436
437 **Table 2. Hi-C Libraries**

Name	mutations	Sample name	valid pairs (M)
Main figures			
wt-0h (G1)		HiC_MJ6_wt_2A_0h	14.5
wt-2h		HiC_MJ6_wt_2A1_2h	27.6
wt-3h		HiC_MJ6_wt_2A_3h	24.1
wt-4h		HiC_MJ6_wt_2A_4h	28
wt-5h		HiC_MJ6_wt_2A1_5h	27.6
wt-6h		HiC_MJ6_wt_2A1_6h	27.6
wt-8h		HiC_MJ6_wt_2A3_8h	19
rec8Δ	*rec8Δ ndt80Δ*	average	
rec8Δ replica 1	*rec8Δ ndt80Δ*	HiC_SSY20_ndt80Drec8D_1A2_8h	39.3
rec8Δ replica 2	*rec8Δ ndt80Δ*	HiC_SSY58_ndt80Drec8D_2A_8h	20.2
ndt80Δ	*ndt80Δ*	average, 8h	
G1	*ndt80Δ*	HiC_SSY14_ndt80D_1A2_0h	36
ndt80Δ-4h	*ndt80Δ*	HiC_SSY14_ndt80D_1A_4h	11.9
ndt80Δ replica 1	*ndt80Δ*	HiC_SSY14_ndt80D_1A1_8h	22.9
ndt80Δ replica 2	*ndt80Δ*	HiC_SSY14_ndt80D_2A2_8h	37
zip1Δ	*zip1Δ ndt80Δ*	average	
zip1Δ replica 1	*zip1Δ ndt80Δ*	HiC_SSY25_ndt80Dzip1D_1B2_8h	22.7

zip1Δ replica 2	zip1Δ ndt80Δ	HiC_SSY25_ndt80Dzip1D_2A_8h	28.6
hop1Δ	hop1Δ ndt80Δ	hop1 ndt80	
hop1Δ replica1	hop1Δ ndt80Δ	HiC_SSY49_ndt80Dhop1D_1A_8h	32.8
Supplementary figures			
wt-2h		HiC_MJ6_wt_3A_2h	22.5
wt-3h		HiC_MJ6_wt_3A_3h	19.8
wt-4h		HiC_MJ6_wt_3A_4h	16.7
wt-6h		HiC_MJ6_wt_3A_6h	37.6

Table 3. Overview of proteins described in this study

Protein	Description
Ndt80	Transcription factor required for exit from pachytene
Rec8	Meiosis-specific kleisin subunit of cohesin
Hop1	Axial element of the synaptonemal complex
Zip1	Transverse filament of the synaptonemal complex

References

1. Zickler, D. & Kleckner, N. Meiotic chromosomes: integrating structure and function. *Annu Rev Genet* **33**, 603-754 (1999).
2. Gray, S. & Cohen, P. E. Control of Meiotic Crossovers: From Double-Strand Break Formation to Designation. *Annu Rev Genet* (2016).
3. Klein, F. et al. A central role for cohesins in sister chromatid cohesion, formation of axial elements, and recombination during yeast meiosis. *Cell* **98**, 91-103 (1999).
4. Sym, M., Engebrecht, J. A. & Roeder, G. S. ZIP1 is a synaptonemal complex protein required for meiotic chromosome synapsis. *Cell* **72**, 365-378 (1993).
5. Smith, A. V. & Roeder, G. S. The yeast Red1 protein localizes to the cores of meiotic chromosomes. *J Cell Biol* **136**, 957-967 (1997).
6. Hollingsworth, N. M., Goetsch, L. & Byers, B. The HOP1 gene encodes a meiosis-specific component of yeast chromosomes. *Cell* **61**, 73-84 (1990).
7. Maleki, S., Neale, M. J., Arora, C., Henderson, K. A. & Keeney, S. Interactions between Mei4, Rec114, and other proteins required for meiotic DNA double-strand break formation in Saccharomyces cerevisiae. *Chromosoma* **116**, 471-486 (2007).
8. Li, J., Hooker, G. W. & Roeder, G. S. Saccharomyces cerevisiae Mer2, Mei4 and Rec114 form a complex required for meiotic double-strand break formation. *Genetics* **173**, 1969-1981 (2006).
9. Dekker, J., Rippe, K., Dekker, M. & Kleckner, N. Capturing chromosome conformation. *Science* **295**, 1306-1311 (2002).

10. Bonev, B. & Cavalli, G. Organization and function of the 3D genome. *Nat Rev Genet* **17**, 661-678 (2016).

11. Merkenschlager, M. & Nora, E. P. CTCF and Cohesin in Genome Folding and Transcriptional Gene Regulation. *Annu Rev Genomics Hum Genet* **17**, 17-43 (2016).

12. Dekker, J. & Mirny, L. The 3D Genome as Moderator of Chromosomal Communication. *Cell* **164**, 1110-1121 (2016).

13. Fudenberg, G., Abdennur, N., Imakaev, M., Goloborodko, A. & Mirny, L. A. Emerging Evidence of Chromosome Folding by Loop Extrusion. *Cold Spring Harb Symp Quant Biol* **82**, 45-55 (2017).

14. Jin, Q., Trelles-Sticken, E., Scherthan, H. & Loidl, J. Yeast nuclei display prominent centromere clustering that is reduced in nondividing cells and in meiotic prophase. *J Cell Biol* **141**, 21-29 (1998).

15. Hayashi, A., Ogawa, H., Kohno, K., Gasser, S. M. & Hiraoka, Y. Meiotic behaviours of chromosomes and microtubules in budding yeast: relocalization of centromeres and telomeres during meiotic prophase. *Genes Cells* **3**, 587-601 (1998).

16. Goloborodko, A., Marko, J. F. & Mirny, L. A. Chromosome Compaction by Active Loop Extrusion. *Biophys J* **110**, 2162-2168 (2016).

17. Gibcus, J. H. et al. A pathway for mitotic chromosome formation. *Science* **359**, (2018).

18. Kakui, Y., Rabinowitz, A., Barry, D. J. & Uhlmann, F. Condensin-mediated remodeling of the mitotic chromatin landscape in fission yeast. *Nat Genet* **49**, 1553-1557 (2017).

19. Lazar-Stefanita, L. et al. Cohesins and condensins orchestrate the 4D dynamics of yeast chromosomes during the cell cycle. *EMBO J* **36**, 2684-2697 (2017).

20. Naumova, N. et al. Organization of the mitotic chromosome. *Science* **342**, 948-953 (2013).

21. Schalbetter, S. A. et al. SMC complexes differentially compact mitotic chromosomes according to genomic context. *Nat Cell Biol* **19**, 1071-1080 (2017).

22. Xu, L., Ajimura, M., Padmore, R., Klein, C. & Kleckner, N. NDT80, a meiosis-specific gene required for exit from pachytene in Saccharomyces cerevisiae. *Mol Cell Biol* **15**, 6572-6581 (1995).

23. Nagano, T. et al. Cell-cycle dynamics of chromosomal organization at single-cell resolution. *Nature* **547**, 61-67 (2017).

24. Muller, H. et al. Characterizing meiotic chromosomes' structure and pairing using a designer sequence optimized for Hi-C. *Mol Syst Biol* **14**, e8293 (2018).

25. Rao, S. S. P. et al. A 3D map of the human genome at kilobase resolution reveals principles of chromatin looping. *Cell* **159**, 1665-1680 (2014).

26. Nora, E. P. et al. Spatial partitioning of the regulatory landscape of the X-inactivation centre. *Nature* **485**, 381-385 (2012).

27. Dixon, J. R. et al. Topological domains in mammalian genomes identified by analysis of chromatin interactions. *Nature* **485**, 376-380 (2012).

28. Ito, M. et al. Meiotic recombination cold spots in chromosomal cohesion sites. *Genes Cells* **19**, 359-373 (2014).

29. Fudenberg, G. et al. Formation of Chromosomal Domains by Loop Extrusion. *Cell Rep* **15**, 2038-2049 (2016).

30. Schwarzer, W. et al. Two independent modes of chromatin organization revealed by cohesin removal. *Nature* **551**, 51-56 (2017).

31. Rao, S. S. P. et al. Cohesin Loss Eliminates All Loop Domains. *Cell* **171**, 305-320.e24 (2017).

32. Wutz, G. et al. Topologically associating domains and chromatin loops depend on cohesin and are regulated by CTCF, WAPL, and PDS5 proteins. *EMBO J* **36**, 3573-3599 (2017).

33. Conrad, M. N., Lee, C. Y., Wilkerson, J. L. & Dresser, M. E. MPS3 mediates meiotic bouquet formation in Saccharomyces cerevisiae. *Proc Natl Acad Sci U S A* **104**, 8863-8868 (2007).

34. Trelles-Sticken, E., Adelfalk, C., Loidl, J. & Scherthan, H. Meiotic telomere clustering requires actin for its formation and cohesin for its resolution. *J Cell Biol* **170**, 213-223 (2005).

515 35. Sun, X. et al. Transcription dynamically patterns the meiotic chromosome-axis interface.
516   *Elife* **4**, (2015).
517 36. Møens, P. B. & Pearlman, R. E. Chromatin organization at meiosis. *Bioessays* **9**, 151-153
518   (1988).
519 37. Marko, J. F. & Siggia, E. D. Polymer models of meiotic and mitotic chromosomes. *Mol Biol*
520   *Cell* **8**, 2217-2231 (1997).
521 38. Blat, Y. & Kleckner, N. Cohesins bind to preferential sites along yeast chromosome III,
522   with differential regulation along arms versus the centric region. *Cell* **98**, 249-259 (1999).
523 39. Crawley, O. et al. Cohesin-interacting protein WAPL-1 regulates meiotic chromosome
524   structure and cohesion by antagonizing specific cohesin complexes. *Elife* **5**, e10851
525   (2016).
526 40. Challa, K., Lee, M.-S., Shinohara, M., Kim, K. P. & Shinohara, A. Rad61/Wpl1 (Wapl), a
527   cohesin regulator, controls chromosome compaction during meiosis. *Nucleic Acids Res*
528   **44**, 3190-3203 (2016).
529 41. Jin, H., Guacci, V. & Yu, H.-G. Pds5 is required for homologue pairing and inhibits
530   synapsis of sister chromatids during yeast meiosis. *J Cell Biol* **186**, 713-725 (2009).
531 42. Petela, N. J. et al. Scc2 Is a Potent Activator of Cohesin's ATPase that Promotes Loading
532   by Binding Scc1 without Pds5. *Mol Cell* **70**, 1134-1148.e7 (2018).
533 43. Haarhuis, J. H. I. et al. The Cohesin Release Factor WAPL Restricts Chromatin Loop
534   Extension. *Cell* **169**, 693-707.e14 (2017).
535 44. Ganji, M. et al. Real-time imaging of DNA loop extrusion by condensin. *Science* (2018).
536 45. Sanborn, A. L. et al. Chromatin extrusion explains key features of loop and domain
537   formation in wild-type and engineered genomes. *Proc Natl Acad Sci U S A* **112**, E6456-
538   65 (2015).
539 46. Nasmyth, K. Disseminating the genome: joining, resolving, and separating sister
540   chromatids during mitosis and meiosis. *Annu Rev Genet* **35**, 673-745 (2001).
541 47. Goloborodko, A., Imakaev, M. V., Marko, J. F. & Mirny, L. Compaction and segregation of
542   sister chromatids via active loop extrusion. *Elife* **5**, (2016).
543 48. Alipour, E. & Marko, J. F. Self-organization of domain structures by DNA-loop-extruding
544   enzymes. *Nucleic Acids Res* **40**, 11202-11212 (2012).
545 49. Tedeschi, A. et al. Wapl is an essential regulator of chromatin structure and chromosome
546   segregation. *Nature* **501**, 564-568 (2013).
547 50. Subramanian, V. V. et al. Persistent DNA-break potential near telomeres increases
548   initiation of meiotic recombination on short chromosomes. *Biorxiv* (2017).
549 51. Thacker, D., Mohibullah, N., Zhu, X. & Keeney, S. Homologue engagement controls
550   meiotic DNA break number and distribution. *Nature* **510**, 241-246 (2014).
551 52. Kerpedjiev, P. et al. HiGlass: web-based visual exploration and analysis of genome
552   interaction maps. *Genome Biol* **19**, 125 (2018).
553

554 # Methods

555 **Yeast strains and cell culture growth.**

556 Strains used in this study were derived from SK1 and are listed in Table 1.

557 **Monitoring meiotic progression by flow cytometry and quantification of nuclear divisions**

558 Cells were fixed in 70% EtOH, digested with 1 mg/ml RNAse (10 mM Tris-HCl pH 8.0, 15 mM
559 NaCl, 10 mM EDTA pH 8.0) for 2 h at 37 ˚C, 800 rpm and subsequently treated with 1 mg/ml
560 Proteinase K in 50 mM Tris-HCl pH 8.0 at 50 ˚C, 800 rpm for 30 min for analysis by FACS. Cells
561 were then washed in 50 mM Tris-HCl pH 8.0 and stained in the same buffer with 1 uM Sytox
562 green overnight in the fridge. FACS profiles were plotted with R using the library *hwglabr2*
563 (https://github.com/hochwagenlab/hwglabr2). Fixed cells were also used for quantification of
564 nuclear divisions by spreading onto a microscope slide, mounting with Fluoroshield containing
565 DAPI followed by analysis with a Zeiss Scope.A1 microscope.

566 **Hi-C library preparation**

567 The Hi-C protocol used was amended from[1] by ~5-fold reduction in all materials and volumes.
568 Briefly, *S. cerevisiae* diploid cells were synchronised in G1 by growth at 30 ˚C for ~15 h in 30
569 ml YPA (1% Yeast extract, 2% Peptone, 1% K-acetate) to OD600 of ~4, harvested, washed,
570 and resuspended in prewarmed sporulation medium (2% KAc with 0.2x nutritional supplements)
571 before fixing 5 ml aliquots (20-30 ODs) of relevant timepoints with formaldehyde at 3% final
572 concentration for 20 min at 30 °C, 250 rpm, then quenched by incubating with a final
573 concentration of 0.35 M Glycine (2x the volume of Formaldehyde added) for an additional 5
574 minutes. Cells were washed with water, split into two samples and stored at -80˚C ready for
575 library preparation. Cells were thawed, washed in spheroplasting buffer (SB, 1 M Sorbitol, 50
576 mM Tris pH 7.5) and digested with 100 ug/ml 100T Zymolyase in SB containing 1% beta-
577 Mercaptoethanol for 15-20 min at 35 ˚C. Cells were washed in restriction enzyme buffer,
578 chromatin was solubilised by adding SDS to 0.1% and incubating at 65 ˚C for 10 minutes.
579 Excess SDS was quenched by addition of Triton X100 to 1%, and chromatin was incubated with
580 2.07U/ul of *Dpn*II overnight at 37 ˚C. DNA ends were filled in with nucleotides, substituting dCTP
581 for biotin-14-dCTP using Klenow fragment DNA polymerase I at 37 ˚C for 2 h followed by
582 addition of SDS to 1.5% and incubation at 65 ˚C for 20 min to inactivate Klenow and further
583 solubilise the chromatin. The sample volume was diluted 15-fold, crosslinked DNA ends ligated
584 at 16 ˚C for 8 h using 0.024U/ul of T4 DNA ligase, and crosslinks reversed by overnight
585 incubation at 65 ˚C in the presence of Proteinase K. DNA was precipitated with ethanol,

586   dissolved in TE and passed through an Amicon 30 kDa column. DNA was further purified by

587   phenol:chloroform:isoamylalcohol extraction and precipitated again before treating with

588   RNaseA at 37 ˚C for 1 h. Biotin was removed from unligated ends by incubation with T4 DNA

589   polymerase at 20˚C for 4 h and at 75 ˚C for 20 min for inactivation of the enzyme. DNA was

590   subsequently fragmented using a Covaris M220 (Duty factor 20%, 200 cycles/burst, 350s, 20

591   ˚C), and DNA ends were repaired and A-tailed using T4 DNA polymerase, T4 Polynucleotide

592   Kinase and Klenow fragment DNA polymerase I before isolating fragments of 100-250 bp using

593   a Blue Pippin (Sage). Biotinylated fragments were enriched using streptavidin magnetic beads

594   (C1) and NextFlex (Bioo Scientific) barcoded adapters were ligated while the DNA was on the

595   beads. Resulting libraries were minimally amplified by PCR and sequenced using paired end

596   42 bp reads on a NextSeq500 (Illumina; Brighton Genomics).

Hi-C data processing and analysis

598   Hi-C sparse matrices were generated at varying spatial resolutions using the Hi-C-pro pipeline[2],

599   using a customised S288c reference genome (*SK1Mod*, in which high confidence SK1-specific

600   polymorphisms were inserted in order to improve read alignment rates; manuscript in

601   preparation) and plotted using R Studio (version 1.0.44) after correcting for read depth

602   differences between samples. Raw read statistics are presented in **Table 2**. Repeat biological

603   samples gave broadly similar matrices and, unless indicated otherwise, were averaged to

604   improve their expected quantitative accuracy. As visual inspection indicated a number of

605   potential translocations in the SK1 strain as compared with the S288c reference genome, for

606   conservative downstream analyses, additional bins were masked if they contained potential

607   translocations. Such bins were identified if they either had values in *trans* at the level of the

608   median of the third diagonal in *cis*, or the maximum value in *trans* exceeded the maximum value

609   in *cis* for SSY14 for bins displaying these properties in either *ndt80Δ-0h* or in *ndt80Δ-8h* and for

610   MJ6 in *wt-0h* or *wt-4h*. chr1 was excluded from downstream analysis as few informative bins

611   remained after filtering potential translocations.

612

613   Average maps centered at centromeres and telomeres were calculated as in[3], ensuring that

614   collected patches for average centromere maps did not extend inter-chromosomally, and

615   collected patches for average telomere maps did not extend beyond centromeres or inter-

616   chromosomally. Contact frequency versus distance curves, *P(s),* were calculated from 2 kb

617   binned maps, with logarithmically-spaced bins in *s* (numutils.logbins, https://bitbucket.org /

618   mirnylab/mirnylib, start =2, end = max(binned arm lengths), N=50), and restricting the

619   calculation to bin pairs within chromosomal arms and excluding bins less than 20 kb from

620   centromeres or telomere (as in[3]), and normalized to the average value at 4 kb. *P(s)* stratified by

621   distance to telomeres was calculated using the combined distance to telomeres for each bin-

622   pair (as in[4]), and excluded bins-pairs where one bin was closer to a centromere than telomere

623   along that arm. Distance to centromeres, and *P(s)* stratified by this distance, was calculated

624   similarly. Log2 insulation profiles were calculated using a sliding diamond window (as in[5]) with

625   a +/-20 kb (+/-10 bins) extent; as in[6] downstream analyses were restricted to when there were

626   zero or one filtered bins in the sliding window. To calculate histograms of cis/total (**Fig. 2D**),

627   bins were defined as either Rec8 or non-Rec8. To calculate *P(s)* split by Rec8 bin-pair status,

628   each bin-pair (i.e. entry of the heatmap) was assigned as either Rec8-Rec8, Rec8-nonRec8, or

629   non-non (e.g. **Fig. 2E**). *P(s)* was then aggregated separately across chromosomes for these

630   three categories, similar to calculation of *P(s)* within and between TADs[7]. Average log2

631   observed/expected maps were calculated by first dividing by intra-arm *P(s)* and then averaging

632   together appropriate patches of Hi-C maps. Correlations between Rec8 occupancy from[8] and

633   insulation or cis/total profiles excluded chromosome 12 because the rDNA locus greatly alters

634   the insulation profile within the right arm of the chromosome.

Polymer simulations

636   Meiotic loop extrusion simulations begin with a generic polymer representation of the yeast

637   chromatin fiber similar to that used in previous models of yeast mitotic chromosomes[9], where

638   each 20 nm monomer represents 640 bp (~4 nucleosomes). We simulated the chromatin fiber

639   with excluded volume interactions and without topological constraints, using Langevin dynamics

640   in OpenMM, as in[10,11]. Importantly, meiotic simulations remove the geometric constraints

641   specific to the Rabl conformation[12,13] because this is not visible in meiotic pachytene *ndt80Δ* Hi-

642   C maps. As our focus was to characterize the grids of intra-chromosomal interactions, we

643   considered a system with multiple copies of chromosome 13, equivalent to four copies of the

644   haploid genome in terms of total genomic content (4 x 13 copies of chromosome 13), to enable

645   efficient computational averaging of simulated Hi-C maps. Extruded loops were generated

646   according to parameters that describe the dynamics of loop extruders, using the simulation

647   engine described in[14]: extruder *separation*, extruder *processivity*, chromatin fiber *relaxation time*

648   relative to extruder velocity, and *barrier strength*. Because yeast chromosomes are short

649   compared to higher eukaryote chromosomes, relaxation time is relatively rapid and we focused

650   on *separation, processivity,* and *barrier strength*. At every given timepoint an extruded loop is

651   realized as a bond between monomers at the two bases of the loop (see

652   ./src/examples/loopExtrusion in https://bitbucket.org/mirnylab/openmm-polymer/).

654   Upon encountering a barrier, a loop extruder is paused with probability according to the barrier

655   strength; barrier strength =1 indicates an impermeable barrier, barrier strength =0 indicates no

impediment to extrusion. We assume loop extrusion occurs independently on each chromatid, and simulate loop extrusion dynamics on a 1D lattice (as in[7]) where the number of lattice sites equals the total number of monomers (75,140). Bi-directional barriers were placed at monomers with positions corresponding to Rec8 ChIP-seq sites[8], and pause extruders according to the barrier strength parameter. We assume a uniform birth probability, constant death probability, and that all barriers have an equal strength; as additional data becomes available, these assumptions can be relaxed and more detailed models can be built.

We investigated scenarios where chromatids are then either left individualized (52 copies), crosslinked to sisters (26 pairs), or additionally paired with homologs (13 pairs-of-pairs). For simulations with sister crosslinks, these were added (following[15]) when extruded loop bases were present at cognate positions ±30 monomers (~20kb) on both chromatids (distance=20nm); homolog crosslinks were added similarly when sister crosslinks were present on both chromatids (distance=100nm); centromeres and telomeres were always paired, and both presented impermeable (strength=1) boundaries to extruders. To avoid introducing pseudo-knots, if extruded loops were nested only the outer cohesins were considered as possible bases for sister crosslinks, sister crosslinks were only allowed between the same side of loop bases (i.e. left-to-left arm or right-to-right arm), and sister crosslinks were only added between bases at the reciprocal minimum distance.

For calculation of simulated Hi-C maps, contacts were recorded from conformations of the full system, which includes intra- and inter-sister, and interhomologue contacts. Because experimental Hi-C here does not distinguish either sisters or homologs, contacts were then aggregated into one simulated map. For each model and parameter set we investigated, we collected an ensemble of conformations, generated simulated chr13 Hi-C maps, and compared their features and *P(s)* with those from experimental Hi-C maps. Each simulated chr13 map represented an average over 5400 conformations. *P(s)* for chr13 was calculated from 2kb binned simulated maps exactly as for experimental maps. Maps of goodness-of-fit between simulations and experimental data (e.g. **Fig. 3b,c**) were computed as the geometric standard deviation of the ratio of simulated to experimental *P(s)* combined across $P^{Rec8-Rec8}(s)$, $P^{Rec8-non}(s)$, and $P^{non-non}(s)$, as was previously done for P(s) within TADs of multiple sizes and between TADs[7], for *s* from 10kb to 300kb. This measure reflects the typical fold-deviation for *P(s)*.

Simulated ChIP-seq profiles (**Extended Data Fig. 6b**) for Rec8 were generated by aggregating the position of extruded loop bases (two per extruded loop) across conformations. Statistics of extruded loop positioning relative to Rec8 sites was calculated with *loopstats.py* in *looplib*

692 (https://github.com/golobor/looplib), and arc diagrams (**Extended Data Fig. 6c**) with *loopviz.py*.

693 Conformations showing chromatids or positions of extruded loop bases were rendered in

694 PyMOL (https://pymol.org/sites/default/files/pymol.bib).

695
696
697

698 # References (Methods)

699

700 1. Belton, J. M. & Dekker, J. Hi-C in Budding Yeast. *Cold Spring Harb Protoc* **2015**, 649-661
701 (2015).
702 2. Servant, N. et al. HiC-Pro: an optimized and flexible pipeline for Hi-C data processing.
703 *Genome Biol* **16**, 259 (2015).
704 3. Hsieh, T. S., Fudenberg, G., Goloborodko, A. & Rando, O. J. Micro-C XL: assaying
705 chromosome conformation from the nucleosome to the entire genome. *Nat Methods* **13**,
706 1009-1011 (2016).
707 4. Mizuguchi, T. et al. Cohesin-dependent globules and heterochromatin shape 3D genome
708 architecture in S. pombe. *Nature* **516**, 432-435 (2014).
709 5. Crane, E. et al. Condensin-driven remodelling of X chromosome topology during dosage
710 compensation. *Nature* **523**, 240-244 (2015).
711 6. Nora, E. P. et al. Targeted Degradation of CTCF Decouples Local Insulation of
712 Chromosome Domains from Genomic Compartmentalization. *Cell* **169**, 930-944.e22
713 (2017).
714 7. Fudenberg, G. et al. Formation of Chromosomal Domains by Loop Extrusion. *Cell Rep*
715 **15**, 2038-2049 (2016).
716 8. Ito, M. et al. Meiotic recombination cold spots in chromosomal cohesion sites. *Genes Cells*
717 **19**, 359-373 (2014).
718 9. Schalbetter, S. A. et al. SMC complexes differentially compact mitotic chromosomes
719 according to genomic context. *Nat Cell Biol* **19**, 1071-1080 (2017).
720 10. Eastman, P. et al. OpenMM 7: Rapid development of high performance algorithms for
721 molecular dynamics. *PLoS Comput Biol* **13**, e1005659 (2017).
722 11. Eastman, P. & Pande, V. S. Efficient nonbonded interactions for molecular dynamics on
723 a graphics processing unit. *J Comput Chem* **31**, 1268-1272 (2010).
724 12. Wong, H. et al. A predictive computational model of the dynamic 3D interphase yeast
725 nucleus. *Curr Biol* **22**, 1881-1890 (2012).
726 13. Tjong, H., Gong, K., Chen, L. & Alber, F. Physical tethering and volume exclusion
727 determine higher-order genome organization in budding yeast. *Genome Res* **22**, 1295-
728 1305 (2012).
729 14. Fudenberg, G. & Imakaev, M. FISH-ing for captured contacts: towards reconciling FISH
730 and 3C. *Nat Methods* **14**, 673-678 (2017).
731 15. Goloborodko, A., Imakaev, M. V., Marko, J. F. & Mirny, L. Compaction and segregation of
732 sister chromatids via active loop extrusion. *Elife* **5**, (2016).
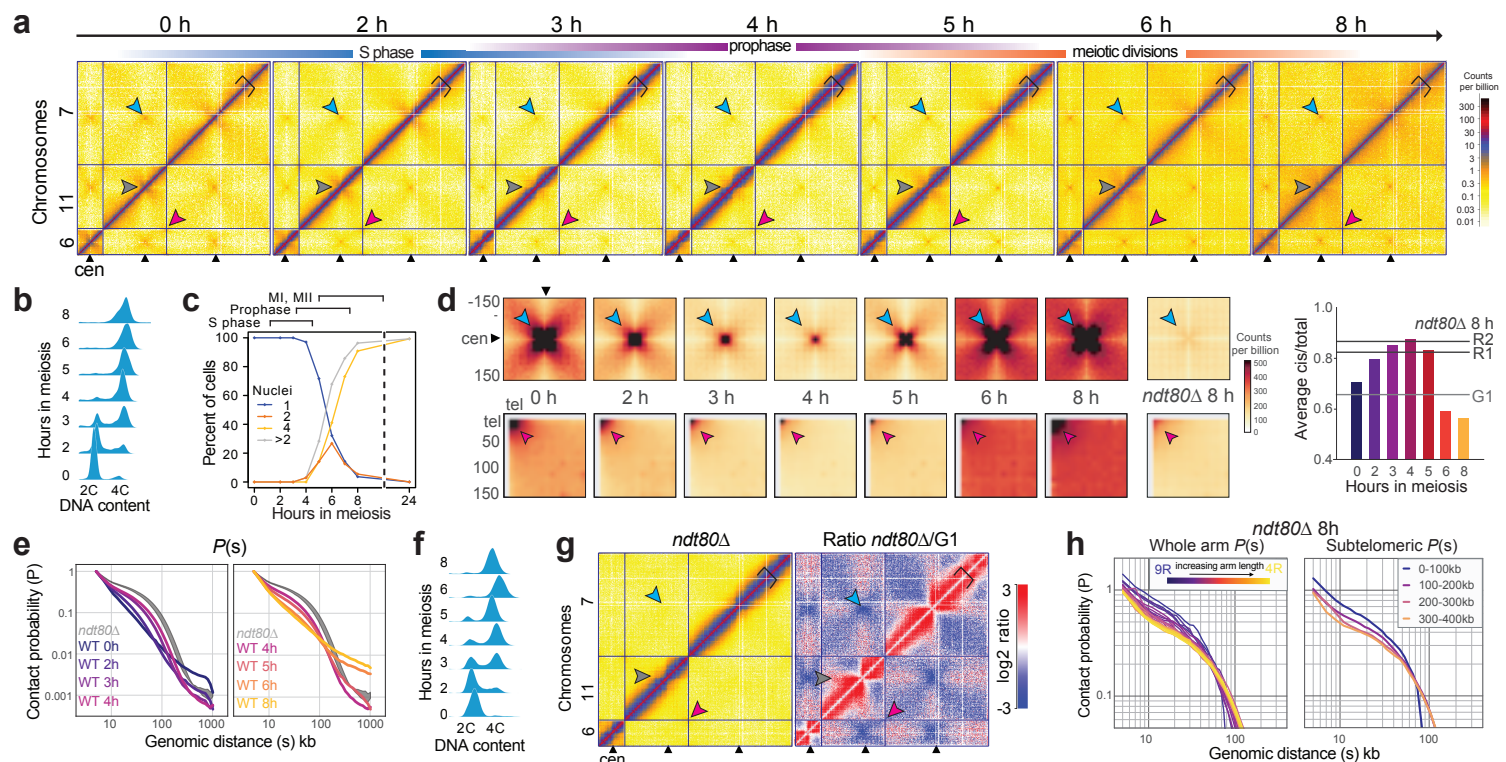
733

Figure 1

Figure 1. Chromosome conformation during yeast meiosis.

a. Cells were collected during meiosis at indicated timepoints and analysed by Hi-C. At 0h the cells are in G1. Representative Hi-C contact maps of chromosomes 6, 11, and 7 plotted at 5 kb resolution. Centromeres, telomeres and arm fold-back at the centromere are indicated by blue, red and grey arrows, respectively, and axial compaction by the width of the main diagonal relative to the fixed-width black clamp. For interactive HiGlass[52] views see: http://higlass.pollard.gladstone.org/app/?config=Z5iwKpjzQpePCXXyvuYGeQ

b. Meiotic entry assessed by FACS; at 4 h, the majority of cells show a 4C peak indicating completion of DNA replication.

c. Meiotic progression was monitored by quantification of nuclear divisions determined by DAPI staining. Around 4 h, cells start to undergo meiotic divisions I and II. The majority of cells undergo meiotic divisions between 4 and 8 h, indicating the degree of heterogeneity within the cell population.

d. *Upper panels*: Average *trans* centromere-centromere contact maps. *Lower panels*: *trans* telomere-telomere contact maps. *Right*: ratio of *cis* to total contact frequency.
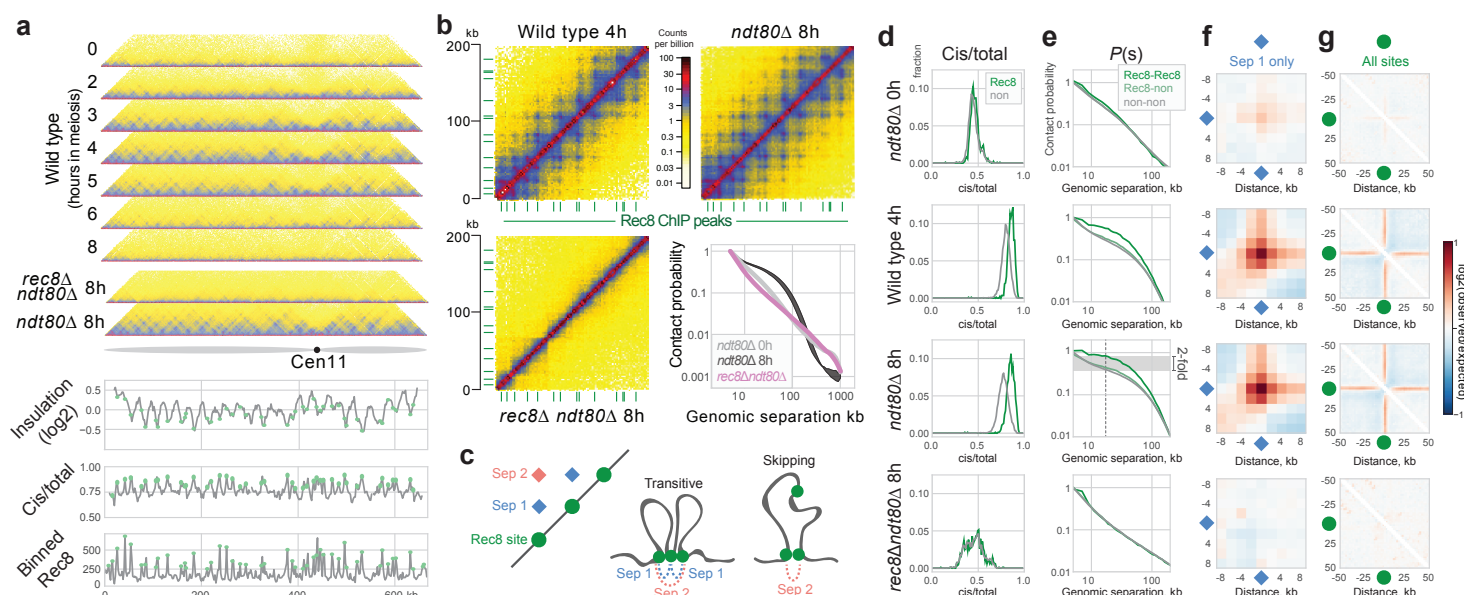
e. Intra-arm contact probability versus genomic distance, *P(s),* indicating the emergence (*left*) and disappearance (*right*) of chromosome arm compaction during meiosis. Shaded area bounded above and below by the two *ndt80Δ* 8h replicates.

f. Meiosis was induced in *ndt80Δ* cells for 8h and meiotic entry was checked by monitoring DNA replication by FACS.

g. *ndt80Δ* cells were grown for 8h in sporulation media and analysed by Hi-C (*left*). Log2 ratio of *ndt80Δ* cells 8h over G1 (*right*). Centromeres and telomeres are indicated by blue and red arrows, respectively, and axial compaction by a black clamp.

h. *Left*: Contact probability of individual chromosome arms stratified by length. *Right*: Contact probability stratified by the distance from the telomere.
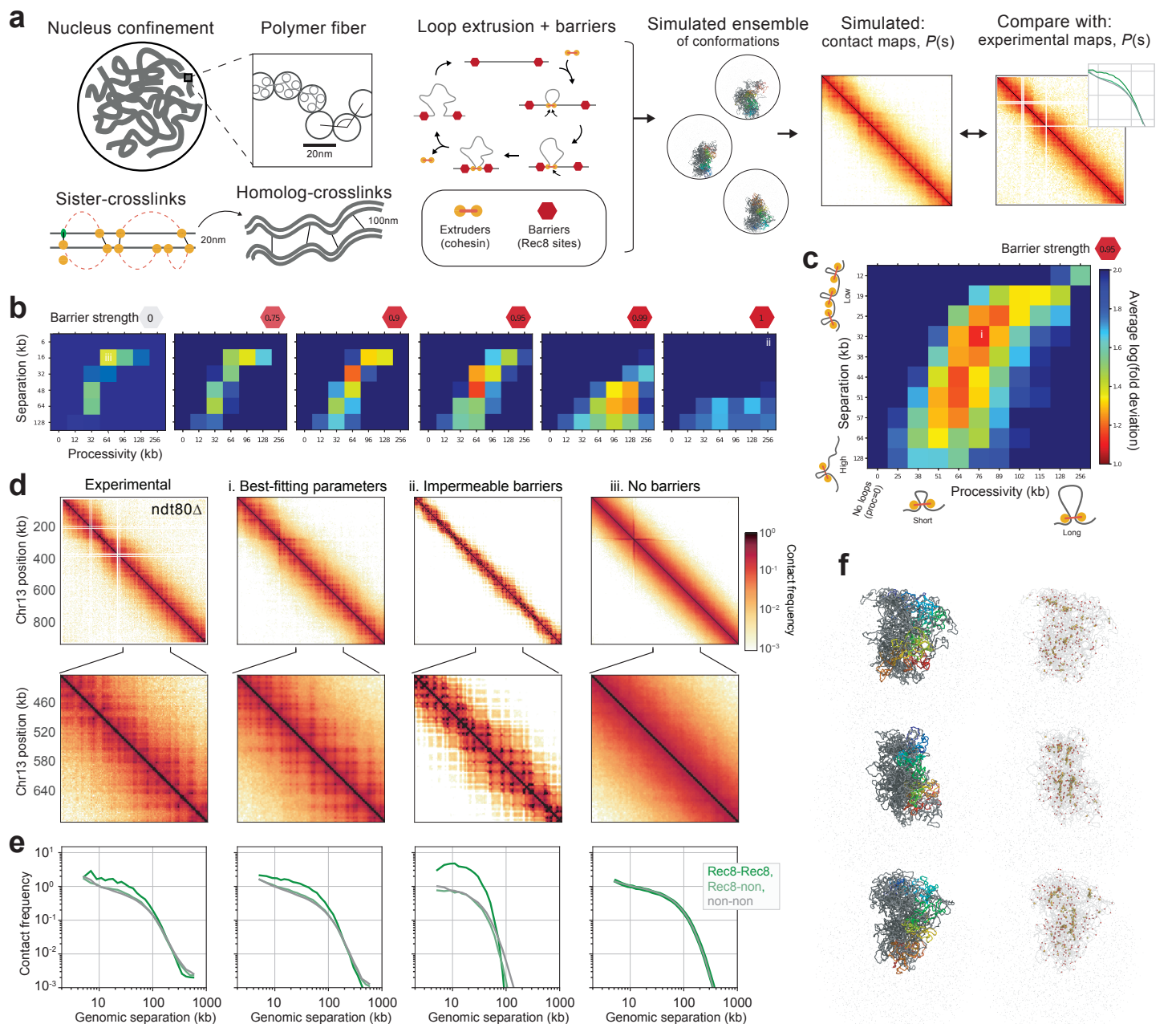
Figure 2

Figure 2. Emergence of a Rec8-dependent grid of punctate interactions in meiosis

a. Hi-C contact maps of chromosome 11 for the indicated genotypes plotted at 2 kb bin resolution, showing near-diagonal interactions. Wild type timepoints as in **Fig. 1a**. **Lower panels**: log2(insulation); cis/total ratio, Rec8 ChIP-seq[28], all binned at 2kb. Insulation and cis/total calculated from *ndt80Δ* maps. Positions of Rec8 sites indicated as green circles. Genome-wide cis/total (Spearman's R=0.62, P<1e-10) and insulation (R= -0.23, P<1e-10, insulation window = 20 kb) profiles are correlated with Rec8 occupancy.

b. Zoom-in into contact maps on chromosome 11 (0-200kb) of wt-4h and *ndt80Δ* (top) and *rec8Δ* (*bottom left*). Contact probability versus genomic distance, *P(s)*, for G1(*ndt80Δ-0h*) and *ndt80Δ* and *rec8Δ* (*bottom right*). Data shown is the average (n=2) except for wt-4h. Rec8 peak sites called from ChIP-seq data[28] are indicated in green. For an interactiveview see: http://higlass.pollard.gladstone.org/app/?config=Twrh61jGT4SlxotaguTlJg

c. Simplified illustration of how a grid of peaks on a Hi-C map can emerge between Rec8 sites either by transitive contacts between adjacent loops, or by loops that skip over adjacent sites. Experimentally observed grids extend much further than separation=2 (**Extended Data Fig. 4c**)

d. Cis/total ratios for Rec8 (green) and nonRec8 (grey) sites for indicated datasets.

e. Contact frequency versus distance between Rec8-Rec8 sites (green), Rec8-nonRec8 sites (light green) and nonRec8-nonRec8 sites (green).

f. Log2 ratio of contact frequency between adjacent Rec8-sites (separation=1) compared to average cis interactions.

g. Log2 ratio of contact frequency centered at Rec8 sites compared to average cis interactions.

In *ndt80Δ*, Rec8 sites show: elevated cis/total frequency (0.85 versus 0.77), elevated pairwise contact frequency (~2-fold at 20 kb), and mild insulation. These distinctions are similar in wild type pachytene (4h) yet absent in G1 (*ndt80Δ-0h*) or in *rec8Δ*.

Figure 3

Figure 3. Model for meiotic chromosome compaction in prophase.
a. In simulations, yeast chr13 was represented as a polymer fiber confined to the nucleus subject to additional meiosis-specific constraints. These include: extruded loops, sister crosslinks, and homolog crosslinks (**Methods**). Barriers to extruded loops were placed at Rec8 sites[28]. We imposed inter-sister and inter-homologue crosslinks at sites of extruded loop bases in order to approximate the paired arrangement of homologues at pachytene (**Extended Data Fig. 6**). For each set of extruded loop parameters (*processivity, separation,* and *barrier strength*), conformations were collected and used to generate simulated contact maps. These were then compared with experimental contact maps via the combined average fold discrepancy with *P(s)* curves for Rec8-Rec8, Rec8-non, and non-non bin pairs at 2 kb resolution.
b. Goodness-of-fit for indicated barrier strengths over coarse grids of processivity and separation demonstrate that intermediate barrier strengths are required to agree with experimental *ndt80Δ* Hi-C maps.
c. Goodness-of-fit for a fine grid of processivity versus separation at barrier strength 0.95. Best-fitting models had separation ~32kb and processivity ~76kb, corresponding to ~60% coverage of the genome by extruded loops of average length 26kb.
d. From *left* to *right*: contact maps for chr13 for *ndt80Δ*, and simulations with (i) best-fitting parameters, (ii) relatively stable loops between neighboring Rec8 sites, and (iii) no barriers.
e. P(s) split by Rec8-Rec8, Rec8-non, and non-non, as in **Fig. 2d**.
f. Conformations for best-fitting simulations, which highlight: (*left*) one chromatid colored from start (red) to end (blue); (*right*) extruders (yellow), extrusion barriers (red), and extruders paused at barriers (orange).
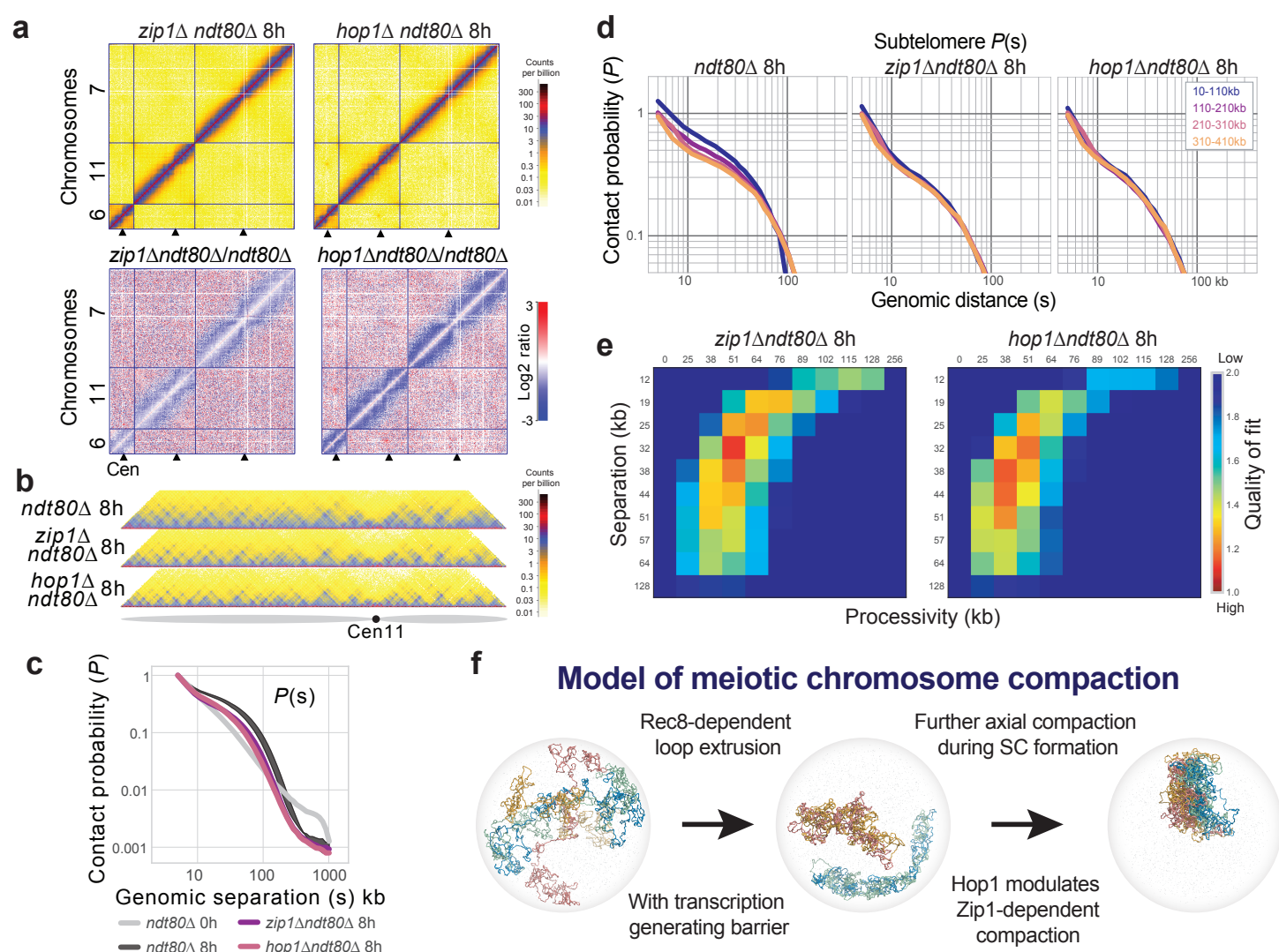
Figure 4

Figure 4. Hop1 and Zip1-dependent compaction of Rec8-dependent loops.
a. *Top*: Hi-C maps for *hop1Δ* and *zip1Δ* (plotted as in **Fig. 1a)**. *Bottom*: Log2 ratio of hop1Δ over *ndt80Δ* (as in **Fig. 1g)**. For interactive views of the full genome, see http://higlass.pollard.gladstone.org/app/?config=TTBGu5DDR0SHAa09zrjTXA
**b.** Hi-C contact maps of chromosome 11 for *hop1Δ* and *zip1Δ* plotted at 2kb bin resolution, showing near-diagonal interactions, as in **Fig. 2a**.
c. Contact probability versus genomic distance for G1, *ndt80Δ*, *hop1Δ*, *zip1Δ*. Shaded area bounded above and below by *ndt80Δ* replicas. Average between two replicas for *zip1Δ* and one sample for G1 and *hop1Δ* are shown.
d. Contact probability over genomic distance averaged over all chromosome arms stratified by distance from the telomere.
e. Goodness-of-fit for simulations without homolog crosslinks with a fine grid of processivity versus separation at barrier strength 0.95 *zip1Δ* and *hop1Δ*.
f. Model of meiotic chromosome compaction: Rec8-dependent loop formation leads to initial chromosome arm compaction and emergence of a grid-like pattern of Hi-C interactions that jointly agrees with a mechanism of loop extrusion including barrier elements. We suggest that transcription could impose such barriers. Hop1 and Zip1 are dispensable for this step, but are required for synapsis, where additional compaction occurs differentially along chromosome arms.

Extended Data Figure 1
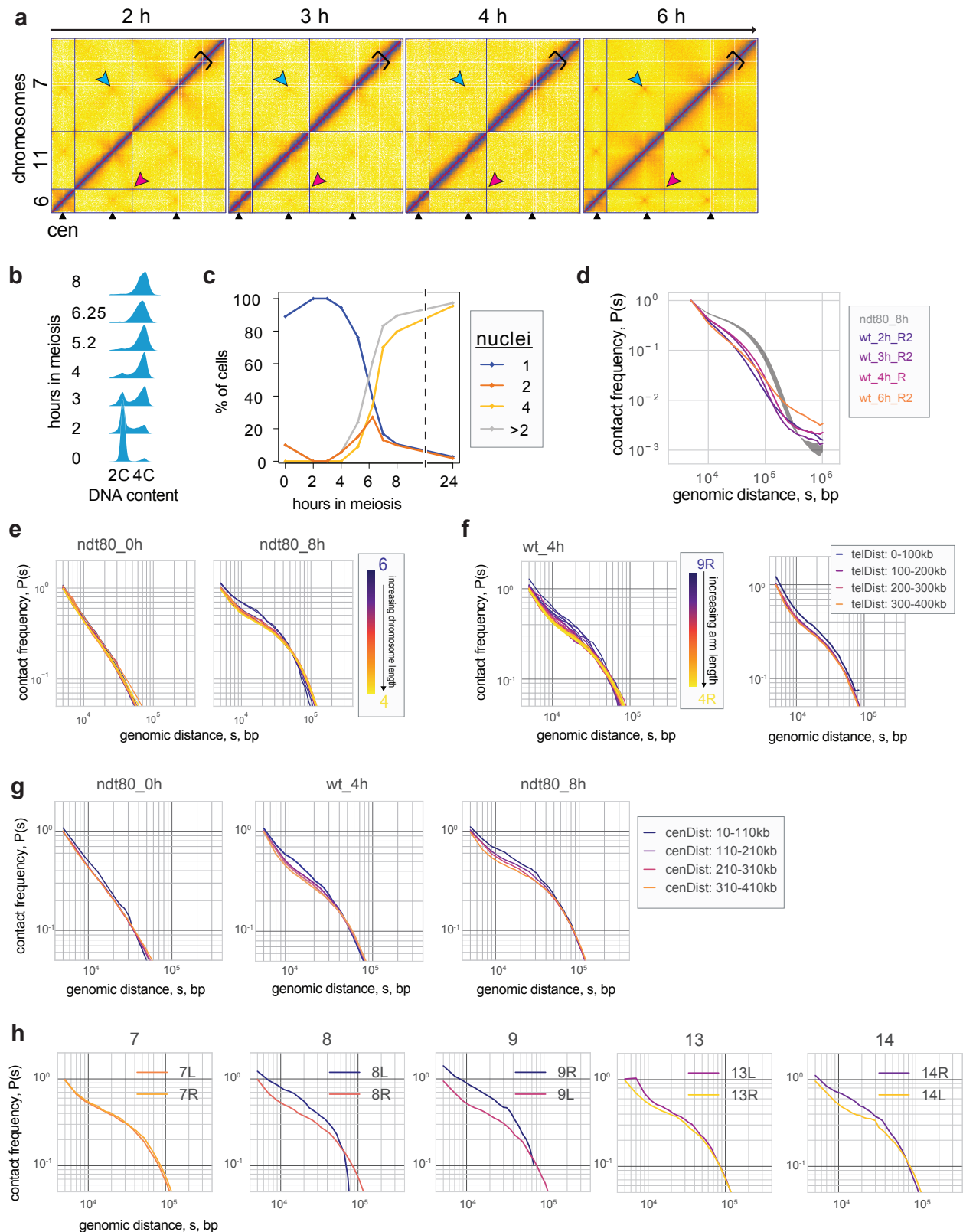
Extended Data Fig. 1

a-d. Results from a replicate timecourse, collected and characterized independently of the timecourse in Fig. 1.

a. Hi-C maps, plotted as in Fig. 1a.

b. FACS as in Fig. 1b.

**c.** DAPI as in Fig. 1c.

d. *P(s)* as in Fig. 1e.

e. *P(s)* for chromosomes stratified by size for *ndt80Δ*-0h, *ndt80Δ*-8h. Short chromosomes display relatively elevated *P(s)* at short distances, and an earlier shoulder.

f. *Left*: *P(s)* for individual chromosome arms, stratified by size for wt-4h. Short arms display relatively elevated *P(s)* at short distances, and an earlier roll-over. *Right*: Intra-arm *P(s)* stratified by the distance from the telomere for wt-4h, averaged across all chromosomes. Telomere-proximal regions display elevated *P(s)* at short distances.

g. Intra-arm *P(s)* stratified by the distance from the centromere for G1 (*ndt80Δ*-0h), *wt*-4h, *ndt80Δ*-8h, averaged across all chromosomes.

h. Contact probability of single chromosome arms for *ndt80Δ*-8h.
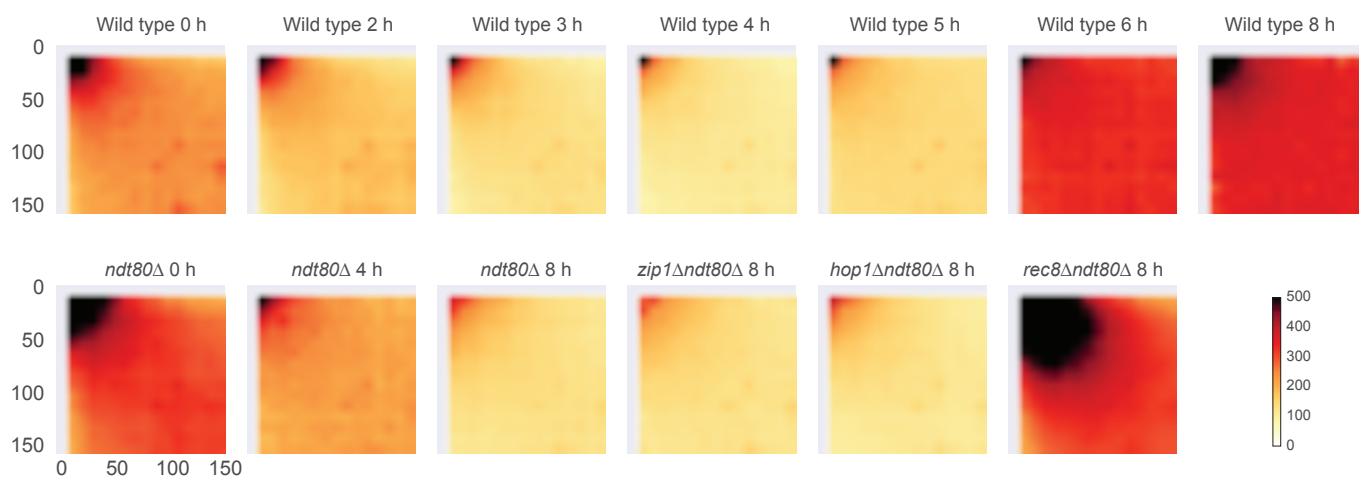
Extended Data Figure 2

a Trans cen-cen
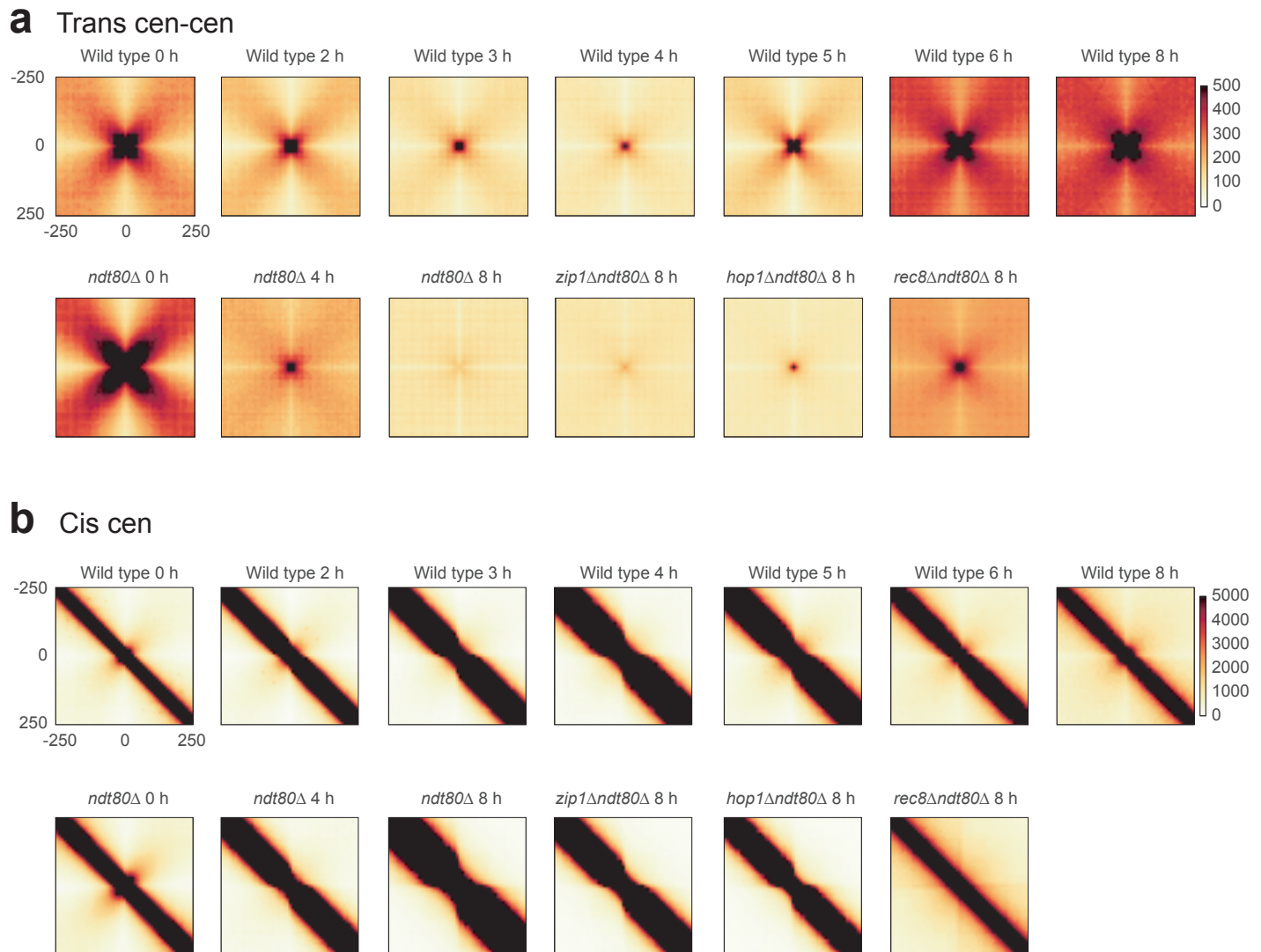
b Cis cen

Extended Data Fig. 2
a. Average *trans* centromere-centromere contact maps for indicated data sets.
b. Average *cis* centromere-centromere contact maps for indicated data sets. Note the loss of the folding back in meiosis, and how the intra-arm enrichment is insulated at centromeres in meiosis.
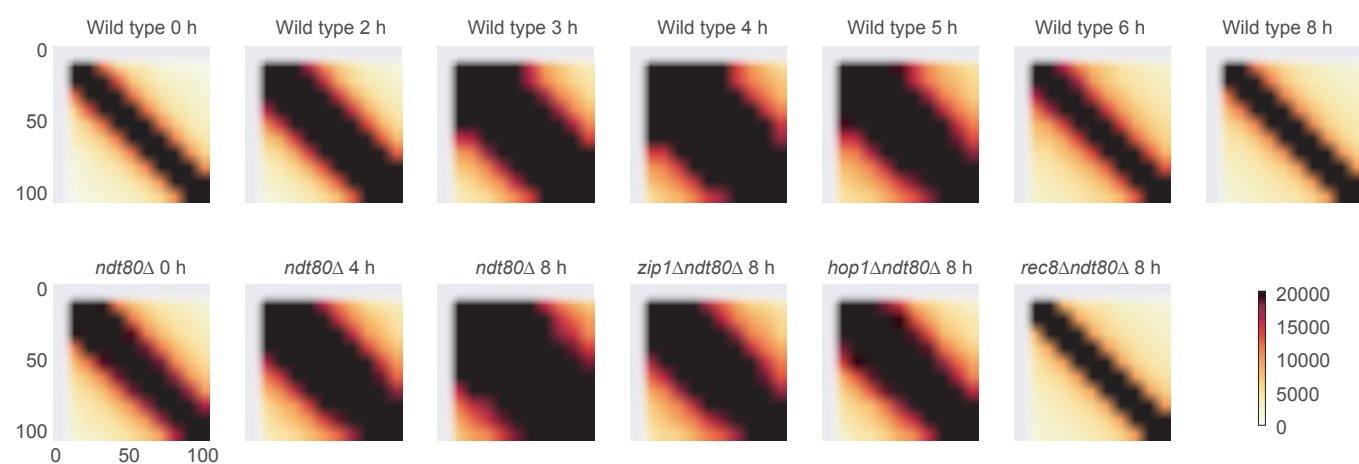
Extended Data Figure 3

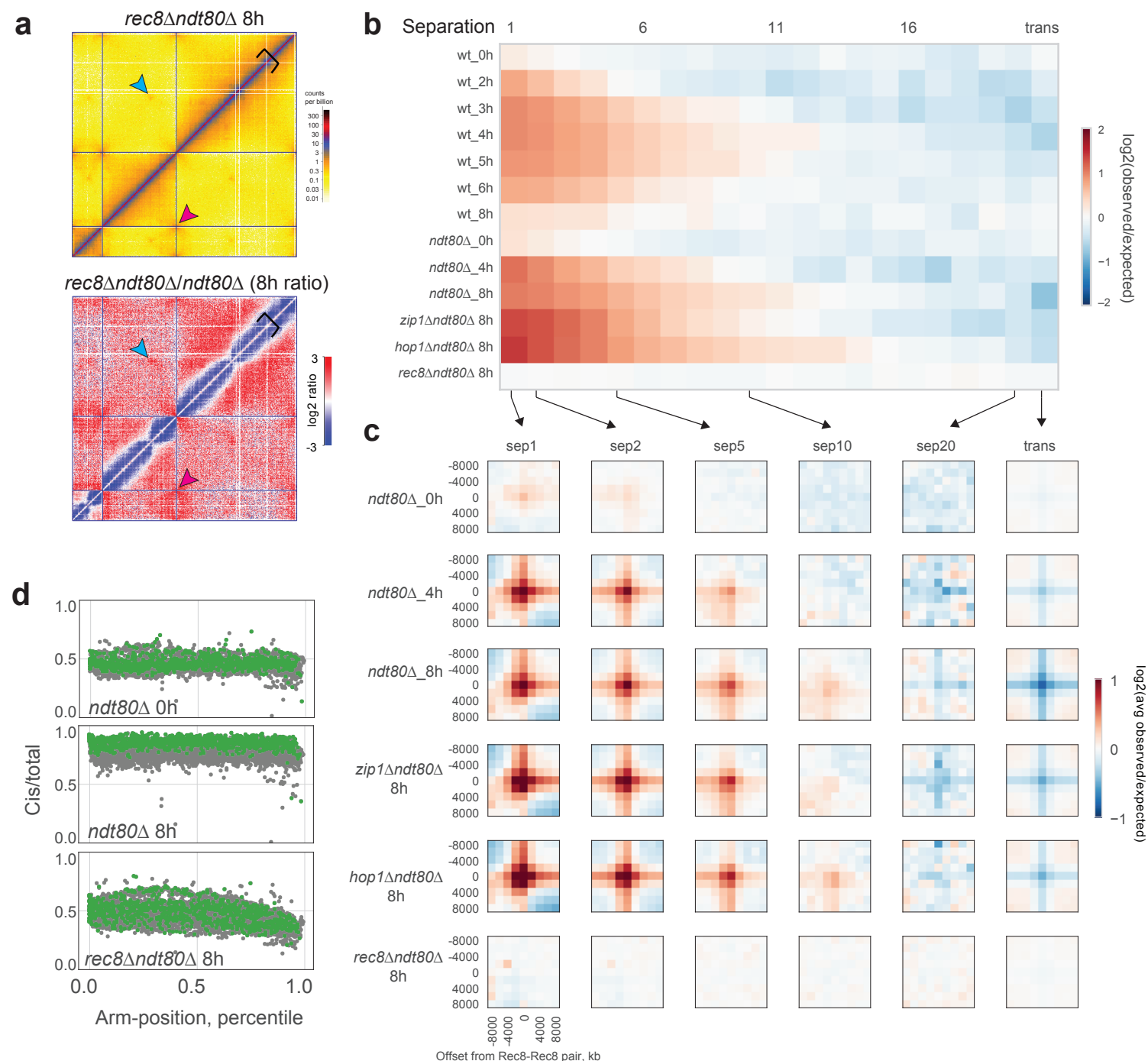**Extended Data Fig. 3**
a. Average *trans* telomere-telomere contact maps for indicated datasets.
b. Average telomere-telomere contact maps between the two telomeres of the same chromosome.
c. Average contact map around each telomere in *cis.*
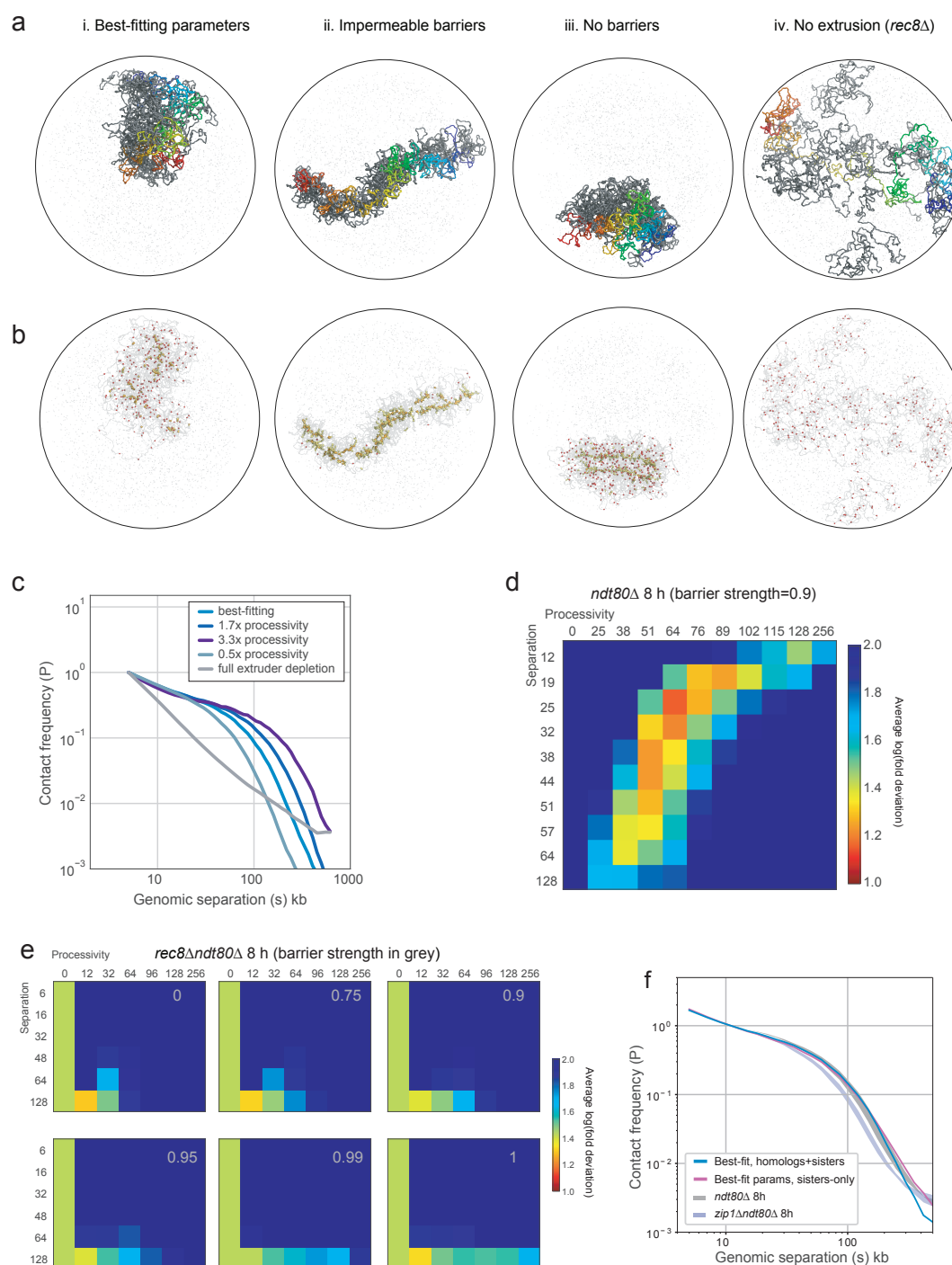
Extended Data Figure 4

Extended Data Fig. 4
a. *Left*: Hi-C contact maps of *rec8Δ ndt80Δ*. Chromosomes 6, 11 and 7 are shown as representatives for the whole genome. *Right*: Log2 Hi-C ratio maps of *rec8Δ ndt80Δ / ndt80Δ*. Plotted as in Fig. 1g.
b. Log2 observed over expected contact frequency at Rec8-Rec8 peak pairs as a function of separation across datasets.
c. Log2 observed over expected contact frequency +/-8 kb around Rec8-Rec8 peak pairs at the indicated separations. Together, **b-c** demonstrate that Rec8-Rec8 enrichments are strongest between adjacent sites, decrease between non-adjacent sites with increasing genomic separation, and are absent in *trans*. Equally important, these meiotic features are lost in *rec8Δ*. As for mammalian interphase, this observation in meiosis argues for a *cis*-acting process underlying the formation of focal interactions between Rec8 sites.
d. cis/total as a function of distance along the chromosomal arm, Rec8 sites marked in green.

Extended Data Figure 5

Extended Data Fig. 5

a. Representative conformation for the indicated parameter sets. As in **Fig. 3F,** one chromatid from a homologous quartet of chromatids coloured from start to end according to the spectrum; other three coloured in grey.
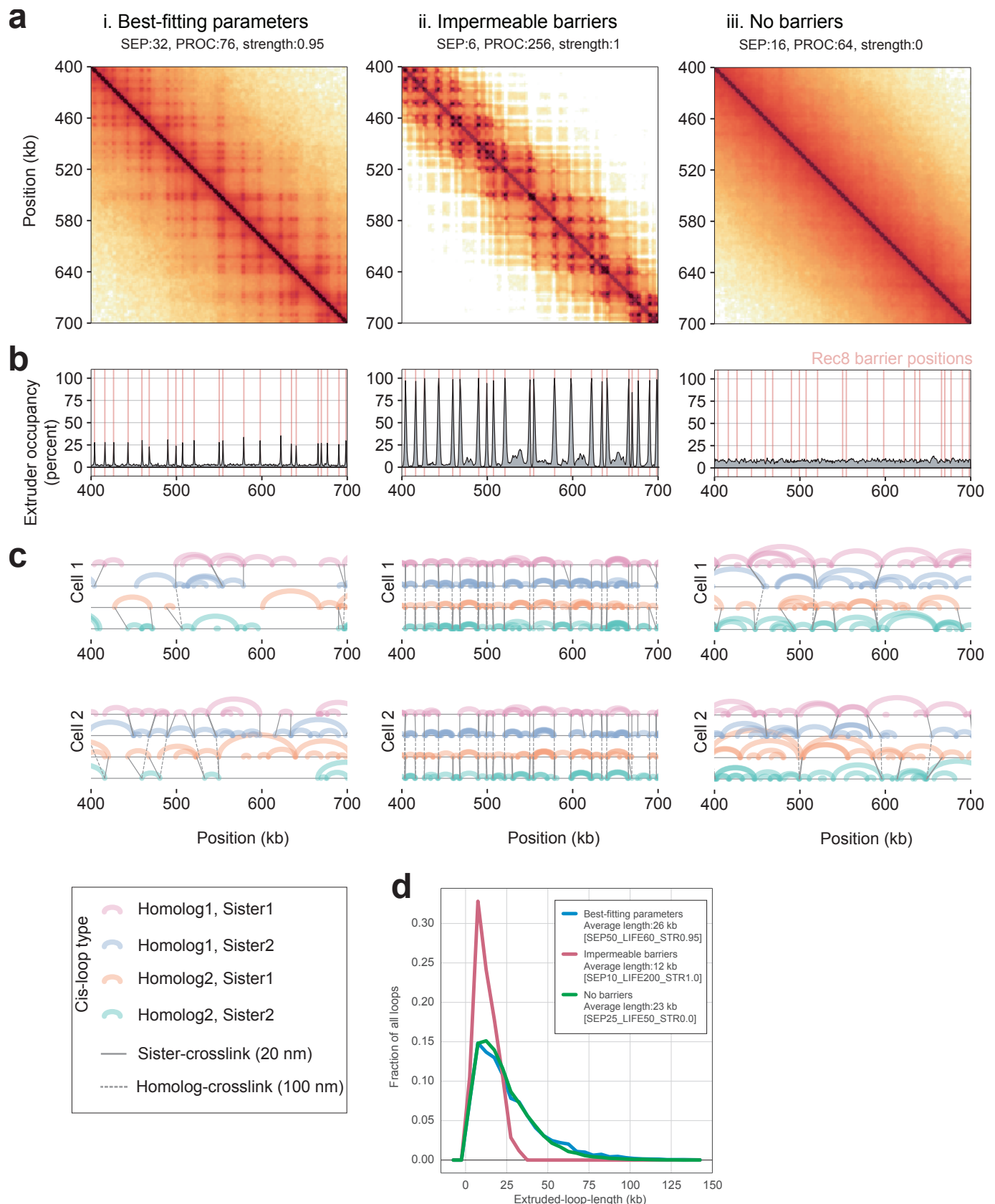
b. For the same three conformations, positions of Rec8 sites indicated with red spheres, positions of extruded loop bases in yellow, and extruders overlapping a Rec8 site in orange. Note the stable loops between neighbouring Rec8 sites creates a very elongated chromatid (ii). Also note the majority of Rec8 sites are unoccupied in (iii), despite the self-assembly of two axial cores and a strong brush. Finally, note very dispersed chromosomes in (iv), consistent with EM[3] for *rec8Δ*.

c. Contact frequency versus distance, *P(s),* for indicated simulations. Note that the loss of the shoulder in *P(s)* in the case of full extruder depletion mirrors the difference between experimental *ndt80Δ* and *rec8Δ* Hi-C maps. Simulations with increased processivity predict that *P(s)* would shift rightward if unloading was impaired, as could happen in *waplΔ.* Conversely, if unloading was enhanced, simulations with decreased processivity indicate a leftward shift in P(s), until the absence of extruders.

d. Goodness-of-fit for a fine grid of processivity versus separation at barrier strength 0.90. The best-fit occurs at similar processivity and separation as for barrier strength 0.95 shown in **Fig. 3c**, but with slightly lower goodness-of-fit.

e. Goodness-of-fit to *rec8Δ* data for simulations with the indicated barrier strengths (in grey: 0.00, 0.75, 0.90, 0.95, 0.99, 1.00) over coarse grids of processivity and separation demonstrates that the best fits have few if any extruded loops, regardless of barrier strength.

f. *P(s)* curves for simulations with sisters and homologs with the best-fitting parameters for *ndt80Δ-8h* maps compared to P(s) for simulations with sisters only show that simply removing homolog tethering does not recapitulate the sort of shifted P(s) seen experimentally in *zip1Δ* Hi-C.

Extended Data Figure 6

Extended Data Fig. 6
a. Simulated contact maps for the indicated region of chr13 for: (i) best-fitting simulations, (ii) simulations with relatively stable loops between neighboring Rec8 sites (barrier strength=1 and high processivity), and (iii) no barriers, as in **Fig. 2d.**
b. Simulated ChIP-seq profiles for the indicated region of chr13. Best-fitting simulations (i) display occupancy well below 100% at Rec8 sites. Simulations with stable loops (ii) display highly occupied Rec8 sites. Simulations without barriers (iii) have homogenous Rec8 occupancy across the genome.
c. Positions of extruded loops (arcs) sister crosslinks (solid black lines) and homolog crosslinks (dashed lines) for four chromatids in two separate cells, showing how the simulated Hi-C maps and ChIP-seq profiles emerge from the stochastic positioning of extruded loops from cell-to-cell. For statistics, see **Supplementary Table S1**.
d. Histogram of extruded loop lengths for indicated parameters (i, ii, iii).